Petrological Investigations and Zircon U-Pb Dating of High Pressure Felsic Granulites from the Yushugou Complex, South Tianshan, China

ZHANG Lu[1], ZHANG Lifei[1,*], ZHU Jianjiang[1], XIA Bin[2], LÜ Zeng[1] and Thomas BADER[1]

1 *The Key Laboratory of Orogenic Belts and Crustal Evolution, School of Earth and Space Sciences, Peking University, Beijing 100871, China*

2 *State Key Laboratory of Geological Processes and Mineral Resources, College of Earth Sciences, China University of Geosciences, Wuhan 430074, China*

Abstract: As a window of insight into the lower crust, high pressure granulite has received much attention since last decade. Yushugou high pressure granulite-peridotite Complex was located in the northeast margin of Southern Tianshan, NW China. Previous ideas agreed that the peridotite unit in Yushugou, combined with the ultramafic rocks in Tonghuashan and Liuhuangshan, represent an ophiolite belt. However, the metamorphic evolution and tectonic mechanism of the Yushugou high pressure (HP) granulite remain controversial. Petrological investigations and phase equilibrium modelling for two representative felsic granulite samples suggest two stages metamorphism of the rocks in Yushugou Complex. Granulite facies metamorphism (Stage I) with P-T conditions of 9.8–10.4 kbar at 895–920°C was recorded by the porphyroblastic garnet core; HP granulite facies metamorphism (Stage II) shows P-T conditions of 13.2–13.5 kbar at 845–860°C, based on the increasing grossular and decreasing pyrope contents of garnet rims. The Yushugou HP felsic granulites have recorded an anti-clockwise P-T path, characterized by the temperature decreasing and pressure increasing simultaneously. The LA-ICP-MS isotopic investigations on zircons from the felsic granulite show that the protolith ages of the granlulites are ~430 Ma, with two age groups of ~390 Ma and 340–350 Ma from the metamorphic rims of zircon, indicating the Stage I and II metamorphic events, respectively. A tectonic model was proposed to interpret the processes. The investigated felsic granulite was derived from deep rooted hanging wall, with Stage I granulite facies metamorphism of ~390 Ma, which may be related to the Devonian arc magmatic intrusion; Stage II HP granulite facies metamorphism (340–350 Ma) may due to the involvement of being captured into the subducting slab and experienced the high pressure metamorphism.

Key words: Anticlockwise P-T path, HP felsic granulites, P-T pseudosection, U-Pb zircon dating, South Tianshan

1 Introduction

As a window of insight into the lower crust, high grade metamorphic granulite has received more and more attention since it was first proposed by Green and Ringwood (1967) (Carswell and O'Brien, 1993; Smithies and Bagas, 1997; Appel et al., 1998; Wei Chunjing et al., 2001; O'Brien and Rötzler, 2003; Wei Chunjing, 2012). The geothermal gradient of the high pressure granulite is 18–22 °C/km, which belongs to medium-pressure facies series and represents the normal to a little thickened middle or lower crust setting (Zhai Mingguo, 2009; Wei Chunjing, 2012). The sequential sequence of metamorphic stages defining the P-T paths in such granulites can place strong constraints on possible tectonic models (Harley, 1989; Guo et al., 2002).

Yushugou high pressure granulite unit lies in the northeastern margin of South Tianshan block and accompanied by peridotite unit (Fig. 1). Because of their unique contact relationship, their origin has been debated for a long time. Previous studies show that the peridotite unit in Yushugou, combined with the ultramafic rocks in Tonghuashan and Liuhuangshan, represents an ophiolite

* Corresponding author. E-mail: lfzhang@pku.edu.cn

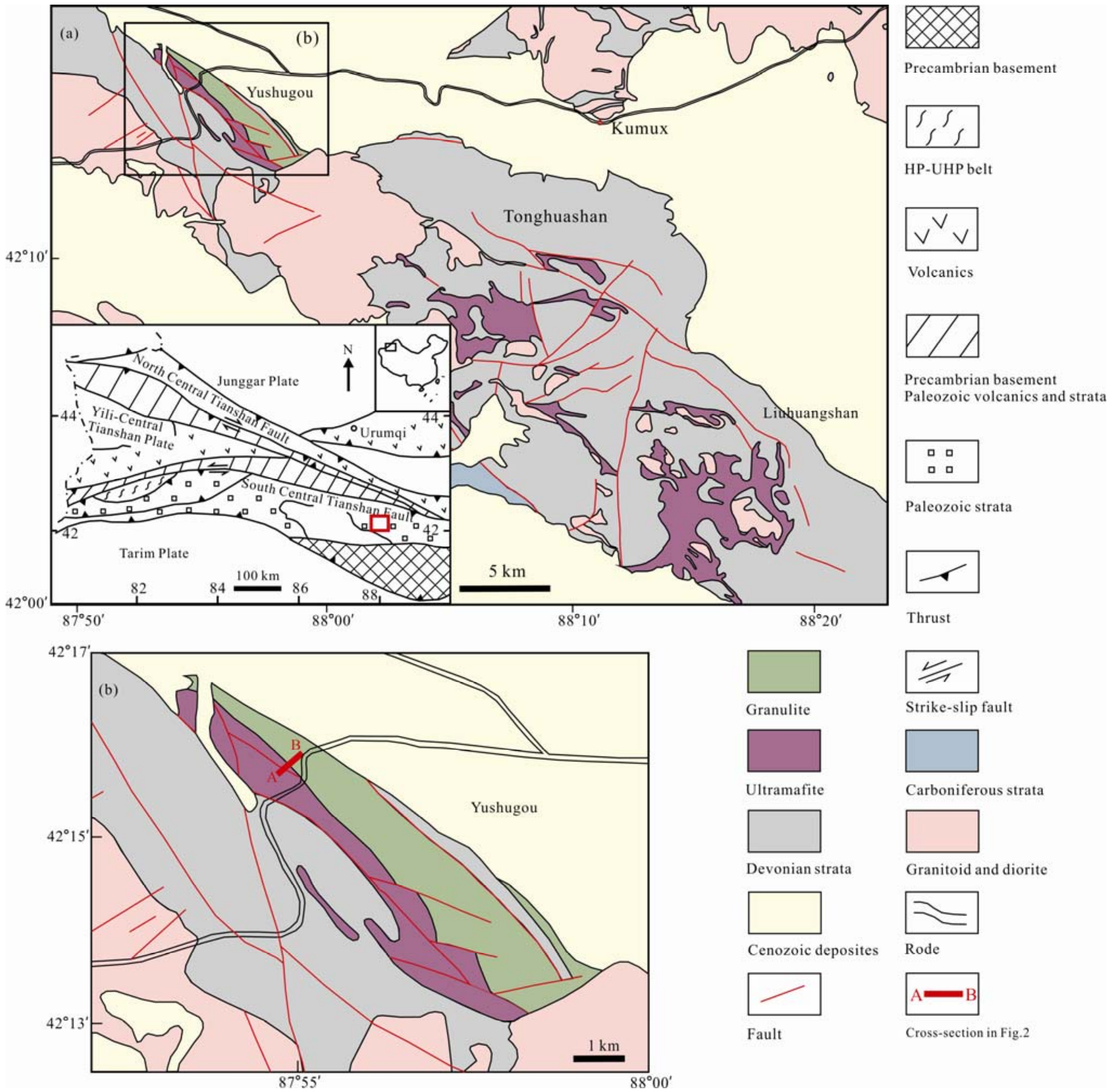

Fig. 1. Simplified geological map of the eastern part of Chinese South Tianshan.
(a) Geological map of Chinese South Tianshan, Xinjiang Uygur Autonomous Region (modified from Lü et al., 2012; XBGMR, 1959, 1960). The Yushugou granulite-peridotite complex is composed by granulite unit and peridotite unit. The ultramafites are distributed in three adjacent places: Yushugou, Tonghuashan and Liuhuangshan. (b) The red solid line (from A to B) represents the cross section in Yushugou show in Fig.2.

belt (Wu Wenkui et al., 1992; Wang Runsan et al., 1999a; Wang Juli et al., 1999; Xu Xiangzhen et al., 2011; Yang Jingsui et al., 2011). However, the petrogenesis of the granulite unit is still in debate (Shu Liangshu et al., 1996; Wang Runsan et al., 1999a; Yang Jingsui et al., 2011; Ji Shaocheng et al., 2014; Zhang et al., 2016). Three different ideas of the tectonic setting of the co-existence HP granulite and peridotite have be raised: (1) They may represent a complete ophiolite suite (Wang Juli et al., 1999; Wang Runsan et al., 1999a; Wang Yan et al., 1999; Zhou et al., 2004); (2) they were tectonic mélange (Shu Liangshu et al., 1996; Li Tianfu et al., 2011; Yang Jingsui et al., 2011); (3) they were formed at continental curst-mantle transition zone, then exhumated to the surface together through sheering action (Ji Shaocheng et al., 2014; Zhang et al., 2016). Compared to the well studied mafic granulite, the metamorphic conditions and tectonic mechanism of the felsic granulites are poorly explored because of lacking appropriate thermobarometry. In previous studies, the calculated peak P-T conditions of the mafic granulite from Yushugou are 800–870°C and 8.8–11.3 kbar (Shu Liangshu et al., 2004); the peak P-T conditions of the high pressure granulite facies (Grt-Di-Pl ± Qz assemblage) and the medium pressure granulite facies (Grt-Opx-Di-Pl-Qz assemblage) are 795–964°C, 9.7–14.2 kbar (Wang et al., 1999b) and 724–826°C, 6.4–8.8 kbar (Li Tianfu et al., 2011) respectively. Zhang et al. (2016) proposed that the felsic granulite underwent UHT (T > 930°C) and HP (10.5–14.5 kbar) metamorphism, which may record a possible prograde process characterized by heating and burial. The granulite-facies metamorphic age are Sm-Nd isochron age of 315 ± 3.62 Ma (Wang et al., 1999b), zircon SHRIMP U-Pb ages of 392 ± 7 Ma and 390 ± 11 Ma (Zhou et al., 2004), zircon SHRIMP U-Pb ages of 390–401 Ma (for the medium pressure granulite facies) (Li Tianfu et al., 2011), ^{40}Ar-^{39}Ar isochron ages of 368.2 ± 4.8 Ma and 360 ± 10 Ma (for the high pressure granulite facies) and Sm-Nd isochron age of 310 ± 5 Ma (for the medium pressure granulite facies) (Wang Runsan et al., 2003). The Previous studies show that the calculated P-T conditions of Yushugou granulite indicated granulite facies metamorphism, but had a relatively large range. Moreover, many researchers used different methods to study the age of granulite facies metamorphism and the results range from 310–390 Ma. These arguments indicate that the P-T conditions and metamorphic age of the granulites are still in controversial.

In this study, we use petrological study, thermodynamic modeling and LA-ICP-MS zircon U-Pb dating to reveal the metamorphic evolution of two types felsic granulites from the Yushugou granulite-peridotite complex.

2 Geological Setting

The Chinese Tianshan orogenic belt is situated between the Junggar plate and the Tarim plate. It extends westward to Tajikistan, Kyrgyzstan, Kazakhstan and Uzbekistan for more than 2500 km long in central Asia (Fig. 1a). It was formed by the collision of the Tarim plate and the Junggar plate in the Late Palaeozoic (Coleman, 1989; Gao et al., 1998). There are two shear zones that have been recognized in Chinese Tianshan: the South Central Tianshan fault, a significant shear zone separating the Tarim and Yili-central Tianshan plates, which formed in the Late Devonian-Early Carboniferous; and the Late Carboniferous-Early Permian North Tianshan fault which separates the Yili-Central Tianshan plate from the North Tianshan island arc (Windley et al., 1990; Allen et al., 1992). The South Tianshan orogen lies between the Tarim craton to the south and the Kazakhstan-Yili terrane to the north. It was formed by the northward subduction of the Tarim plate underneath the Yili-Central Tianshan plate during the closure of the Paleo-Tianshan ocean at the Late Paleozoic (Gao et al., 1999; Zhang et al., 2001; Zhang et al., 2005; Lü et al., 2008; Han et al., 2011; Huang He et al., 2015).

The Yushugou HP granulite-peridotite complex is located at the east of northern margin of South Tianshan, China, which consists mainly of granulite unit and peridotite unit (Fig. 1). The granulite unit consists mainly of mafic granulite and felsic granulite interbedded with layers and lenses of amphibolite and marble (Fig. 2). There are two type granulites in the granulite unit: the mafic granulite and the felsic granulite. The mafic granulite can be subdivided into three types according to the petrographic characteristics: Type I is orthopyroxene-free granulite with garnet-bearing mineral assemblage, Type II is orthopyroxene and garnet-bearing granulite, Type III is two-pyroxene granulite without garnet (with or without spinel). The felsic granulite was subdivided into two types as Type I is opx-bearing granulite with garnet and Type II is opx-free granulite with garnet. The felsic granulites in this unit are generally massive foliated.

Four felsic granulite samples were selected from the granulite unit for petrological studying, phase equilibrium modelling and zircon U-Pb dating. The locations of these samples are illustrated by the filled red star on the cross-section (Fig. 2).

3 Methods

3.1 Electron-microprobe analyses

Electron-microprobe analyses of minerals were performed with a Jeol JXA-8100 super-probe at the MOE Key Laboratory of Orogenic Belts and Crustal Evolution, Peking University. It was operated at 15 kV acceleration voltage, 10 nA beam current and 2 μm beam size. For calibration, natural and synthetic mineral standards were used. Final results were reduced by the PRZ correction program supplied by the manufacturer. For major elements, the relative analytical uncertainties are <2%. Representative mineral compositions are presented in Table 1.

3.2 XRF analyses

Whole-rock compositions of the samples were obtained using an RIX-2100 X-ray fluorescence (XRF) spectrometer on fused glass discs made of whole-rock powder (<200 mesh) and lithium metaborate at the MOE Key Laboratory of Orogenic Belts and Crustal Evolution, School of Earth and Space Sciences, Peking University. Standard andesite GSR2 was used for calibration. Whole-rock compositions are presented in Table 2.

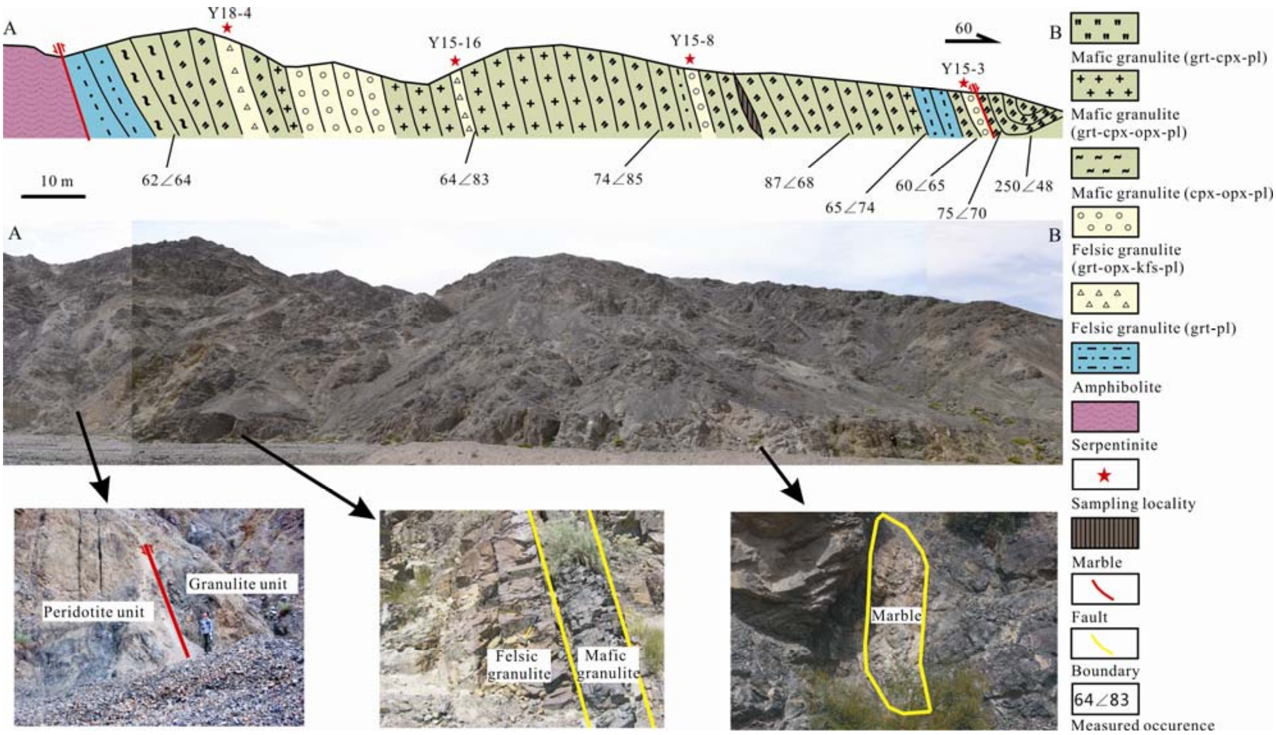

Fig. 2. A cross-section was investigated along the profile A-B in Fig.1b.
The granulite unit consists mainly of mafic granulite and felsic granulite interbedding with layers and lenses of amphibolite and marble. The red stars represent the locations of the four selected samples. Among which, Y15-3 and Y15-8 are Type I felsic granulite, Y15-16 and Y18-4 are Type II felsic granulite. Mineral abbreviations: grt, garnet; cpx, clinopyroxene; pl, plagioclase; opx, orthopyroxene; kfs, K-feldspar.

Table 1 Whole-rock compositions of the granulites Y15-3 and Y15-16 from Yushugou

Samples	SiO_2	Al_2O_3	TiO_2	Fe_2O_3	CaO	MgO	K_2O	Na_2O	MnO	P_2O_5	LOI	Total
XRF analyses (wt%)												
Y15-3	61.03	16.04	1.16	10.23	3.09	4.43	1.88	1.91	0.16	0.06	0.53	100.52
Y15-16	77.27	8.52	0.56	7.13	1.64	2.77	0.41	0.73	0.22	0.02	0.57	99.84
Samples	SiO_2	Al_2O_3	TiO_2	FeO	CaO	MgO	K_2O	Na_2O	O	H_2O	Total	
Stage I bulk-rock compositions (calculated by deducting the calcite composition from the XRF analyses, mol.%)												
Y15-3	65.27	10.11	0.94	8.24	3.45	7.05	1.28	1.98	0.40	1.28	100.00	
Y15-16	80.87	5.26	0.45	5.61	1.81	4.32	0.27	0.74	0.20	0.47	100.00	
Stage II bulk-rock compositions (calculated from mineral modes and microprobe analyses , mol.%)												
Y15-3	67.24	9.93	0.98	6.42	4.11	5.27	1.34	2.47	0.58	1.66	100.00	
Y15-16	81.95	4.99	0.85	4.53	1.97	3.66	0.32	1.12	0.10	0.51	100.00	

LOI, loss on ignition.

3.3 LA-ICP-MS dating

Zircons were prepared by conventional heavy liquid and magnetic techniques and handpicked under a binocular microscope, mounted onto epoxy resin disks and polished to expose the train centers. The choice of analytical sites bases on transmitted and reflected light microscopy to avoid cracks and inclusions and cathodoluminescence (CL) imaging to examine internal structures prior to U-Pb isotopic analysis. CL images were obtained using a Quanta 200F ESEM with a 2-min scanning time at conditions of 15 kV and 120 μA at Peking University. Laser ablation-inductively coupled plasma-mass spectrometry (LA-ICP-MS) U-Pb zircon dating was made by an Agilent 7500ce ICP-MS equipped with an 193 nm excimer laser ablation system (COMPexPro102) at the MOE Key Laboratory of Orogenic Belts and Crustal Evolution, School of Earth and Space Sciences, Peking University. Instrumental conditions and measurement procedures are similar to those described by Yuan et al. (2004). The diameter of the laser spot size was 32 μm. Considering the correction of isotope fractionation effects, zircon Plesovice (337.3 ± 0.4 Ma; Sláma et al., 2008) was used as an external standard and 91500 (1064.1 ± 3.2 Ma; Wiedenbeck et al., 1995) was a monitoring standard. GLITTER 4.4.2 was used to calculate the U-Pb isotopic compositions. Common lead was corrected following the procedure of Andersen (2002). Data processing was done with the ISOPOLT 4.15 (Ludwig, 2003). The results of zircon U-Pb dating are shown in Table 3 and presented on U-Pb concordia plots with 1σ uncertainties in Fig. 9.

Table 2 Representative microprobe analyses of minerals from Y15-3 and Y15-16(unit for oxide is wt%)

	Y15-3										Y15-16					
Mineral	Grt^A-c	Grt^A-r	Grt^B-c	Grt^B-r	Opx^A-c	Opx^A-r	Opx^B	Pl	Kfs	Bt	Grt^A-c	Grt^A-r	Grt^B-c	Grt^B-r	Pl	Bt
SiO_2	38.86	39.25	39.21	39.25	51.34	53.14	52.99	58.70	63.85	38.70	39.06	38.49	38.55	38.81	58.82	37.92
TiO_2	0.01	0.10	0.01	0.00	0.16	0.10	0.07	0.02	0.04	7.65	0.04	0.01	0.09	0.10	0.02	6.10
Al_2O_3	21.84	21.99	21.78	22.80	5.12	2.22	1.76	25.64	18.71	13.44	22.09	21.71	22.24	22.16	25.68	15.12
Cr_2O_3	0.00	0.01	0.08	0.01	0.08	0.10	0.11	0.02	0.00	0.17	0.02	0.02	0.06	0.05	0.00	0.00
Fe_2O_3	2.84	0.17	1.91	0.18	0.00	0.00	0.19	0.07	0.41	0.00	2.39	2.71	1.76	0.54	0.09	0.00
FeO	24.10	25.35	24.76	24.83	20.26	21.50	21.83	0.00	0.00	8.80	23.07	21.82	23.45	23.22	0.00	10.86
MnO	0.69	0.57	0.66	0.61	0.14	0.22	0.17	0.00	0.00	0.04	1.40	1.29	1.24	1.30	0.00	0.04
MgO	10.60	8.76	10.21	9.13	22.45	23.10	23.05	0.03	0.00	17.32	10.76	9.33	10.08	8.83	0.00	15.74
CaO	1.86	4.27	2.55	3.94	0.19	0.24	0.25	7.89	0.30	0.09	2.34	4.79	2.69	4.68	7.81	0.00
Na_2O	0.07	0.00	0.00	0.03	0.05	0.00	0.00	7.46	0.94	0.32	0.01	0.03	0.00	0.05	7.76	0.30
K_2O	0.04	0.00	0.00	0.01	0.01	0.02	0.01	0.38	15.33	9.88	0.01	0.00	0.02	0.00	0.36	9.88
Total	100.61	100.47	100.98	100.77	99.80	100.64	100.41	100.20	99.60	96.42	100.94	99.93	100.00	99.68	100.54	95.97
Oxygen	12.00	12.00	12.00	12.00	6.00	6.00	6.00	8.00	8.00	11.00	12.00	12.00	12.00	12.00	8.00	11.00
Si	2.95	3.00	2.97	2.98	1.89	1.95	1.96	2.63	2.96	2.79	2.95	2.94	2.94	2.98	2.62	2.76
Ti	0.00	0.01	0.00	0.00	0.00	0.00	0.00	0.00	0.00	0.41	0.00	0.00	0.01	0.01	0.00	0.33
Al	1.95	1.98	1.95	2.04	0.22	0.10	0.08	1.35	1.02	1.14	1.97	1.96	2.00	2.01	1.35	1.30
Cr	0.00	0.00	0.01	0.00	0.00	0.00	0.00	0.00	0.00	0.01	0.00	0.00	0.00	0.00	0.00	0.00
Fe^{3+}	0.16	0.01	0.11	0.01	0.00	0.00	0.01	0.00	0.01	0.00	0.14	0.16	0.10	0.03	0.00	0.00
Fe^{2+}	1.53	1.62	1.57	1.58	0.62	0.66	0.67	0.00	0.00	0.53	1.46	1.40	1.50	1.49	0.00	0.66
Mn	0.04	0.04	0.04	0.04	0.00	0.01	0.01	0.00	0.00	0.00	0.09	0.08	0.08	0.09	0.00	0.00
Mg	1.20	1.00	1.15	1.03	1.23	1.27	1.27	0.00	0.00	1.86	1.21	1.06	1.15	1.01	0.00	1.71
Ca	0.15	0.35	0.21	0.32	0.01	0.01	0.01	0.38	0.02	0.01	0.19	0.39	0.22	0.39	0.37	0.00
Na	0.01	0.00	0.00	0.00	0.00	0.00	0.00	0.65	0.09	0.04	0.00	0.00	0.00	0.01	0.67	0.04
K	0.00	0.00	0.00	0.00	0.00	0.00	0.00	0.02	0.91	0.91	0.00	0.00	0.00	0.00	0.02	0.92
Sum	8.00	8.00	8.00	8.00	3.99	4.00	4.00	5.03	5.01	7.70	8.00	8.00	8.00	8.00	5.04	7.73
X_{grs}	0.05	0.12	0.07	0.11							0.06	0.13	0.07	0.13		
X_{prp}	0.41	0.33	0.39	0.35							0.41	0.36	0.39	0.34		
X_{alm}	0.52	0.54	0.53	0.53							0.49	0.48	0.51	0.50		
X_{sps}	0.02	0.01	0.01	0.01							0.03	0.03	0.03	0.03		
X_{an}								0.37							0.36	
X_{Mg}					0.66	0.66	0.65			0.78						0.72

$X_{grs} = Ca/(Ca + Mg + Fe^{2+} + Mn)$, $X_{prp} = Mg/(Ca + Mg + Fe^{2+} + Mn)$, $X_{alm} = Fe^{2+}/(Ca + Mg + Fe^{2+} + Mn)$, $X_{sps} = Mn/(Ca + Mg + Fe^{2+} + Mn)$, $X_{an} = Ca/(Ca + Na)$, $X_{Mg} = Mg/(Mg + Fe^{2+})$. C, core; r, rim. The mineral formulae ferric iron were calculated with the program AX (Holland; http://www.esc.cam.ac.uk/research/research-groups/holland/ax).

4 Petrography and Sample Description

The layered HP felsic granulites from Yushugou are interbedded with mafic granulite and show distinct mylonitic foliation (Fig. 3e). Based on their petrologic characteristics, the felsic granulites can be divided into two types. Type I is opx-bearing felsic granulite (represented by sample Y15-3), which consists mainly of garnet (20–26 vol%), orthopyroxene (1–3 vol%), plagioclase (30–33 vol%), quartz (25–27 vol%) and K-feldspar (7–10 vol%), with minor biotite, rutile and ilmenite (Fig. 3a–b). The garnet can be divided into porphyroblastic garnet (Grt^A, 0.5–1 mm in diameter) and matrix garnet (Grt^B, 50-100 μm in diameter) according to their grain sizes (Fig. 3a–b). The porphyroblastic garnet contains inclusions of orthopyroxene, quartz, plagioclase, biotite, rutile and ilmenite, while the matrix garnet contains quartz, biotite, rutile and ilmenite. The orthopyroxene can also be divided into porphyroblastic orthopyroxene (Opx^A, 0.5–1 mm in diameter) and matrix orthopyroxene (Opx^B, 50–100 μm in diameter) based on their grain sizes (Fig. 3a–b). Small grained garnet were found around the Opx^A (Fig. 3c–d), indicating orthopyroxene being replaced by garnet with the reaction opx + pl = grt + qz. There still exits the intergrowth of garnet and quartz which is probably pseudomorphs after orthopyroxene (Fig. 3f). All these petrographic characteristics described above illustrate two-stage granulite facies metamorphic events. Stage I metamorphism is recorded by the mineral assemblages of GrtA core + Opx^A + pl + bt + ilm + qz (± kfs ± rt), while Stage II metamorphism is recorded by mineral assemblages: GrtA rim/Grt^B ± Opx^B + kfs + pl + bt + rt + ilm + qz.

Type II is opx-free felsic granulite (represented by sample Y15-16), which consists mainly of garnet (12–16%), quartz (60–63%) and plagioclase (14–16%), with minor biotite, rutile, ilmenite (Fig. 3g–h). The garnet can be divided into porphyroblastic garnet (Grt^A, 0.5–1 mm in diameter) and matrix garnet (Grt^B, 50–100 μm in diameter) according to their grain sizes (Fig. 3g–h). The porphyroblastic garnet contains inclusions of quartz, plagioclase, biotite, rutile and ilmenite, while the matrix garnet contains quartz and rutile. All these petrographic characteristics described above illustrate that there exist two-stage metamorphic events. These two stages of metamorphism are recorded by mineral assemblages of GrtA core + pl + bt + ilm + qz (± opx ± rt) and GrtA rim/Grt^B + pl + bt + rt + ilm + qz, respectively.

Table 3 LA-ICP-MS U-Pb analyses of zircons from the granulites and amphibolite in Yushugou

Spot	Position	Th(ppm)	U(ppm)	Th/U	$^{207}Pb/^{206}Pb$	1σ	$^{207}Pb/^{235}U$	1σ	$^{206}Pb/^{238}U$	1σ	ρ	$^{207}Pb/^{235}U$	1σ	$^{206}Pb/^{238}U$	1σ
Granulite Y15-3															
Y15-3-01	meta	39.5	48.8	0.81	0.05281	0.02979	0.44517	0.25010	0.06112	0.00346	0.9	374	176	382	21
Y15-3-02	meta	63.3	63.3	1.00	0.05577	0.02050	0.48325	0.17686	0.06282	0.00263	0.9	400	121	393	16
Y15-3-03	core	28.8	72.0	0.40	0.05407	0.01591	0.51549	0.15062	0.06913	0.00303	0.9	422	101	431	18
Y15-3-04	meta	48.5	58.6	0.83	0.05533	0.01657	0.46802	0.13918	0.06133	0.00259	0.9	390	96	384	16
Y15-3-05	meta	9.7	715.6	0.01	0.05393	0.00269	0.47140	0.02292	0.06337	0.00101	0.9	392	16	396	6
Y15-3-06	meta	108.8	92.1	1.18	0.05564	0.01169	0.48098	0.10025	0.06267	0.00207	0.9	399	69	392	13
Y15-3-07	meta	86.9	85.2	1.02	0.05586	0.01277	0.48098	0.10899	0.06243	0.00230	0.9	399	75	390	14
Y15-3-08	meta	57.5	57.4	1.00	0.05345	0.02651	0.46408	0.22937	0.06295	0.00298	0.9	387	159	394	18
Y15-3-09	meta	42.9	50.3	0.85	0.05551	0.01555	0.47810	0.13301	0.06244	0.00246	0.9	397	91	390	15
Y15-3-10	meta (rim)	49.0	52.2	0.94	0.05365	0.01858	0.40959	0.14105	0.05535	0.00237	0.9	349	102	347	14
Y15-3-11	meta (core)	111.7	142.6	0.78	0.05563	0.00922	0.47392	0.07777	0.06177	0.00173	0.9	394	54	386	11
Y15-3-12	meta	45.9	50.1	0.92	0.05326	0.01808	0.46694	0.15752	0.06356	0.00288	0.9	389	109	397	17
Y15-3-13	rim	84.4	81.5	1.03	0.05380	0.01333	0.46604	0.11457	0.06281	0.00235	0.9	388	79	393	14
Y15-3-14	core	51.6	58.6	0.88	0.05618	0.02132	0.54299	0.20491	0.07008	0.00351	0.9	440	135	437	21
Y15-3-15	meta	85.9	120.7	0.71	0.05370	0.00910	0.47001	0.07907	0.06346	0.00166	0.9	391	55	397	10
Y15-3-16	meta	57.2	59.1	0.97	0.05314	0.01721	0.44894	0.14440	0.06125	0.00280	0.9	377	101	383	17
Y15-3-17	meta	285.1	1977.8	0.14	0.05555	0.00268	0.47865	0.02243	0.06248	0.00097	0.9	397	15	391	6
Y15-3-18	meta	80.1	98.0	0.82	0.05377	0.01150	0.46987	0.09975	0.06336	0.00198	0.9	391	69	396	12
Y15-3-19	meta	56.7	67.6	0.84	0.05594	0.01687	0.48387	0.14492	0.06271	0.00261	0.9	401	99	392	16
Y15-3-20	meta	78.7	82.4	0.95	0.05558	0.01189	0.47940	0.10182	0.06254	0.00193	0.9	398	70	391	12
Y15-3-21	core	149.2	315.8	0.47	0.05655	0.00713	0.54244	0.06779	0.06955	0.00160	0.9	440	45	433	10
Y15-3-22	core	91.9	162.4	0.57	0.05627	0.00804	0.53525	0.07534	0.06897	0.00216	0.9	435	50	430	13
Y15-3-23	meta	86.2	88.2	0.98	0.05187	0.01417	0.39857	0.10820	0.05572	0.00198	0.9	341	79	350	12
Y15-3-24	meta	78.5	84.6	0.93	0.05395	0.01159	0.45910	0.09787	0.06170	0.00202	0.9	384	68	386	12
Y15-3-25	meta	58.2	68.7	0.85	0.05426	0.01443	0.46613	0.12323	0.06229	0.00219	0.9	389	85	390	13
Y15-3-26	core	66.6	251.5	0.26	0.05756	0.00485	0.54152	0.04460	0.06822	0.00154	0.9	439	29	425	9
Y15-3-27	meta	55.4	60.7	0.91	0.05289	0.01604	0.46260	0.13946	0.06342	0.00259	0.9	386	97	396	16
Y15-3-28	rim	100.5	87.8	1.15	0.05305	0.01369	0.46001	0.11801	0.06287	0.00209	0.9	384	82	393	13
Y15-3-29	core	123.3	335.5	0.37	0.05697	0.00692	0.54749	0.06573	0.06968	0.00160	0.9	443	43	434	10
Y15-3-30	meta	57.9	51.1	1.13	0.05572	0.02028	0.47217	0.17075	0.06144	0.00297	0.9	393	118	384	18
Y15-3-31	meta (rim)	104.6	85.5	1.22	0.05487	0.00985	0.42304	0.07497	0.05591	0.00198	0.9	358	53	351	12
Y15-3-32	meta (core)	32.1	41.8	0.77	0.05547	0.01839	0.47531	0.15675	0.06213	0.00254	0.9	395	108	389	15
Y15-3-33	meta (core)	44.2	43.0	1.03	0.05549	0.02119	0.46971	0.17849	0.06137	0.00269	0.9	391	123	384	16
Y15-3-34	meta (rim)	111.9	103.2	1.08	0.05243	0.00988	0.40692	0.07565	0.05628	0.00211	0.9	347	55	353	13
Y15-3-35	meta	56.0	50.6	1.11	0.05455	0.01625	0.46042	0.13607	0.06120	0.00276	0.9	385	95	383	17
Y15-3-36	meta	45.2	57.3	0.79	0.05334	0.01500	0.46027	0.12862	0.06257	0.00230	0.9	384	89	391	14
Y15-3-37	meta	61.9	62.5	0.99	0.05360	0.01173	0.46778	0.10162	0.06328	0.00204	0.9	390	70	396	12
Y15-3-38	meta	75.4	76.1	0.99	0.05550	0.01087	0.47069	0.09130	0.06150	0.00201	0.9	392	63	385	12
Y15-3-39	meta	132.4	327.3	0.40	0.05410	0.00470	0.45779	0.03899	0.06136	0.00127	0.9	383	27	384	8
Y15-3-40	meta	34.3	39.1	0.88	0.05316	0.02082	0.45257	0.17615	0.06173	0.00321	0.9	379	123	386	19
Y15-3-41	meta	66.2	71.4	0.93	0.05536	0.01273	0.47273	0.10773	0.06192	0.00229	0.9	393	74	387	14
Y15-3-42	meta	38.8	49.9	0.78	0.05351	0.01616	0.46815	0.14053	0.06344	0.00244	0.9	390	97	397	15
Y15-3-43	meta	69.5	64.4	1.08	0.05485	0.01394	0.47945	0.12097	0.06339	0.00231	0.9	398	83	396	14
Y15-3-44	meta	79.3	72.4	1.10	0.05347	0.01277	0.46126	0.10911	0.06255	0.00248	0.9	385	76	391	15
Granulite Y15-8															
Y15-8-01	meta	70.9	77.0	0.92	0.05498	0.00258	0.47525	0.02168	0.06268	0.00095	0.9	395	15	392	6
Y15-8-02	meta	36.4	58.4	0.62	0.05358	0.00321	0.46485	0.02735	0.06291	0.00094	0.9	388	19	393	6
Y15-8-03	meta	21.3	31.1	0.69	0.05372	0.00516	0.47145	0.04485	0.06363	0.00113	0.9	392	31	398	7
Y15-8-04	meta	63.8	108.0	0.59	0.05277	0.00200	0.45107	0.01653	0.06198	0.00082	0.9	378	12	388	5
Y15-8-05	meta	69.2	89.0	0.78	0.05535	0.00217	0.47268	0.01798	0.06192	0.00083	0.9	393	12	387	5
Y15-8-06	meta	61.5	65.1	0.94	0.05428	0.00276	0.46666	0.02314	0.06233	0.00095	0.9	389	16	390	6
Y15-8-07	meta	77.9	68.7	1.13	0.05531	0.00304	0.47558	0.02559	0.06235	0.00095	0.9	395	18	390	6
Y15-8-08	meta	22.2	35.0	0.63	0.05500	0.00462	0.47041	0.03898	0.06201	0.00112	0.9	391	27	388	7
Y15-8-09	meta	56.3	65.9	0.85	0.05339	0.00254	0.46092	0.02137	0.06260	0.00092	0.9	385	15	391	6
Y15-8-10	meta	74.0	108.0	0.68	0.05283	0.00197	0.45541	0.01646	0.06251	0.00082	0.9	381	11	391	5
Y15-8-11	meta	33.0	43.8	0.75	0.05318	0.00354	0.45360	0.02966	0.06185	0.00106	0.9	380	21	387	6
Y15-8-12	meta	68.2	130.0	0.52	0.05304	0.00198	0.45033	0.01626	0.06157	0.00082	0.9	378	11	385	5
Y15-8-13	meta	56.0	127.9	0.44	0.05577	0.00212	0.47870	0.01759	0.06224	0.00084	0.9	397	12	389	5
Y15-8-14	meta	58.8	67.8	0.87	0.05548	0.00277	0.47923	0.02338	0.06263	0.00091	0.9	398	16	392	6
Y15-8-15	meta	27.1	39.6	0.68	0.05358	0.00325	0.46779	0.02778	0.06330	0.00109	0.9	390	19	396	7
Y15-8-16	meta	140.2	132.9	1.06	0.05547	0.00230	0.48615	0.01957	0.06356	0.00087	0.9	402	13	397	5
Y15-8-17	meta	287.2	322.7	0.89	0.05479	0.00173	0.47610	0.01446	0.06301	0.00079	0.9	395	10	394	5
Y15-8-18	meta	44.9	44.0	1.02	0.05509	0.00438	0.46896	0.03676	0.06173	0.00107	0.9	390	25	386	6
Y15-8-19	meta	93.0	188.4	0.49	0.05558	0.00231	0.48384	0.01963	0.06312	0.00084	0.9	401	13	395	5
Y15-8-20	meta	46.5	55.1	0.84	0.05522	0.00276	0.48236	0.02357	0.06334	0.00096	0.9	400	16	396	6
Y15-8-21	meta	25.3	71.4	0.35	0.05525	0.00377	0.47731	0.03209	0.06264	0.00098	0.9	396	22	392	6
Y15-8-22	meta	116.4	163.6	0.71	0.05338	0.00187	0.46678	0.01586	0.06340	0.00083	0.9	389	11	396	5
Y15-8-23	meta	23.9	39.7	0.60	0.05535	0.00557	0.47026	0.04679	0.06161	0.00118	0.9	391	32	385	7
Y15-8-24	meta	96.5	85.0	1.14	0.05420	0.00245	0.47698	0.02104	0.06381	0.00093	0.9	396	14	399	6
Y15-8-25	meta	47.8	42.8	1.12	0.05355	0.00325	0.46580	0.02767	0.06307	0.00108	0.9	388	19	394	7
Y15-8-26	meta	51.4	50.2	1.02	0.05560	0.00292	0.48213	0.02477	0.06288	0.00100	0.9	400	17	393	6
Y15-8-27	meta	21.5	37.3	0.58	0.05564	0.00368	0.48056	0.03118	0.06263	0.00107	0.9	398	21	392	6
Y15-8-28	meta	135.9	160.5	0.85	0.05308	0.00190	0.46504	0.01617	0.06352	0.00084	0.9	388	11	397	5

Table 3 Continued

Spot	Position	Th(ppm)	U(ppm)	Th/U	$^{207}Pb/^{206}Pb$	1σ	$^{207}Pb/^{235}U$	1σ	$^{206}Pb/^{238}U$	1σ	ρ	$^{207}Pb/^{235}U$	1σ	$^{206}Pb/^{238}U$	1σ
Y15-8-29	meta	30.6	44.8	0.68	0.05413	0.00344	0.47343	0.02944	0.06342	0.00114	0.9	394	20	396	7
Y15-8-30	meta	24.5	39.3	0.62	0.05321	0.00378	0.46229	0.03228	0.06300	0.00112	0.9	386	22	394	7
Y15-8-31	meta	54.8	67.2	0.82	0.05393	0.00276	0.47152	0.02360	0.06339	0.00100	0.9	392	16	396	6
Y15-8-32	meta	31.7	87.5	0.36	0.05361	0.00257	0.46843	0.02190	0.06335	0.00094	0.9	390	15	396	6
Y15-8-33	meta	48.2	51.0	0.94	0.05518	0.00404	0.47729	0.03448	0.06272	0.00105	0.9	396	24	392	6
Y15-8-34	meta	26.2	259.3	0.10	0.05560	0.00215	0.47890	0.01799	0.06246	0.00084	0.9	397	12	391	5
Y15-8-35	meta	78.7	86.5	0.91	0.05494	0.00257	0.47753	0.02176	0.06302	0.00099	0.9	396	15	394	6
Y15-8-36	meta	22.7	36.5	0.62	0.05336	0.00498	0.46736	0.04315	0.06351	0.00122	0.9	389	30	397	7
Y15-8-37	meta	56.1	101.5	0.55	0.05388	0.00219	0.46935	0.01853	0.06317	0.00091	0.9	391	13	395	6
Y15-8-38	meta	95.8	160.7	0.60	0.05558	0.00202	0.48218	0.01698	0.06291	0.00087	0.9	400	12	393	5
Y15-8-39	meta	61.1	70.1	0.87	0.05536	0.00255	0.47807	0.02142	0.06261	0.00095	0.9	397	15	391	6
Y15-8-40	meta	191.3	253.8	0.75	0.05535	0.00194	0.47861	0.01627	0.06270	0.00085	0.9	397	11	392	5
Y15-8-41	meta	71.7	125.3	0.57	0.05351	0.00220	0.46624	0.01866	0.06317	0.00092	0.9	389	13	395	6
Y15-8-42	meta	174.5	225.2	0.78	0.05586	0.00197	0.48161	0.01648	0.06252	0.00085	0.9	399	11	391	5
Y15-8-43	meta	25.7	36.6	0.70	0.05475	0.00358	0.46761	0.03002	0.06193	0.00108	0.9	390	21	387	7
Y15-8-44	meta	10.7	19.3	0.56	0.05549	0.00779	0.47062	0.06553	0.06149	0.00138	0.9	392	45	385	8
Y15-8-45	meta	230.2	270.3	0.85	0.05315	0.00197	0.46124	0.01657	0.06292	0.00088	0.9	385	12	393	5
Y15-8-46	meta	295.1	671.2	0.44	0.05542	0.00186	0.48181	0.01567	0.06303	0.00083	0.9	399	11	394	5
Y15-8-47	meta	37.8	66.1	0.57	0.05570	0.00293	0.48017	0.02464	0.06250	0.00102	0.9	398	17	391	6
Y15-8-48	meta	52.7	47.0	1.12	0.05639	0.00325	0.47886	0.02703	0.06157	0.00104	0.9	397	19	385	6
Y15-8-49	meta	16.2	30.5	0.53	0.05499	0.00383	0.47426	0.03241	0.06254	0.00116	0.9	394	22	391	7
Y15-8-50	meta	13.6	23.9	0.57	0.05475	0.00438	0.48953	0.03854	0.06483	0.00127	0.9	405	26	405	8
Granulite Y15-16															
Y15-16-01	meta	38.0	42.6	0.89	0.05477	0.01770	0.48835	0.15679	0.06465	0.00283	0.9	404	107	404	17
Y15-16-02	meta	26.4	31.5	0.84	0.05641	0.02094	0.49455	0.18258	0.06357	0.00292	0.9	408	124	397	18
Y15-16-03	meta	55.2	48.7	1.13	0.05607	0.01936	0.49099	0.16844	0.06350	0.00294	0.9	406	115	397	18
Y15-16-04	meta	22.1	31.0	0.71	0.05412	0.02313	0.46302	0.19672	0.06204	0.00338	0.9	386	137	388	21
Y15-16-05	meta	6.2	365.6	0.02	0.05411	0.00384	0.46018	0.03167	0.06168	0.00125	0.9	384	22	386	8
Y15-16-06	meta	4.0	260.9	0.02	0.05314	0.00487	0.40828	0.03655	0.05572	0.00125	0.9	348	26	350	8
Y15-16-07	meta	32.8	35.7	0.92	0.05362	0.01993	0.45091	0.16676	0.06098	0.00266	0.9	378	117	382	16
Y15-16-08	meta	33.1	188.8	0.18	0.05482	0.00551	0.40612	0.04013	0.05372	0.00120	0.9	346	29	337	7
Y15-16-09	meta	9.7	58.8	0.17	0.04990	0.02549	0.43336	0.22063	0.06297	0.00326	0.9	366	156	394	20
Y15-16-10	meta	5.0	141.2	0.04	0.05458	0.00546	0.46191	0.04555	0.06137	0.00128	0.9	386	32	384	8
Y15-16-11	meta	5.9	136.1	0.04	0.05590	0.00707	0.47373	0.05931	0.06145	0.00135	0.9	394	41	384	8
Y15-16-12	meta	8.3	144.7	0.06	0.05431	0.00569	0.40015	0.04128	0.05343	0.00121	0.9	342	30	336	7
Y15-16-13	meta	30.1	35.5	0.85	0.05340	0.03118	0.40832	0.23755	0.05544	0.00303	0.9	348	171	348	19
Y15-16-14	meta	32.0	33.2	0.96	0.05510	0.02968	0.47415	0.25446	0.06240	0.00332	0.9	394	175	390	20
Y15-16-15	meta	25.0	30.6	0.82	0.05489	0.02719	0.48157	0.23742	0.06362	0.00355	0.9	399	163	398	22
Y15-16-16	meta	27.0	33.7	0.80	0.05520	0.02501	0.48712	0.21951	0.06399	0.00355	0.9	403	150	400	22
Y15-16-17	meta	28.1	39.8	0.70	0.05509	0.01991	0.47665	0.17112	0.06274	0.00306	0.9	396	118	392	19
Y15-16-18	meta	4.5	72.2	0.06	0.05517	0.01547	0.48335	0.13474	0.06354	0.00235	0.9	400	92	397	14
Y15-16-19	meta	4.8	144.6	0.03	0.05528	0.01085	0.48976	0.09539	0.06425	0.00186	0.9	405	65	401	11
Y15-16-20	meta	27.4	37.7	0.73	0.05304	0.01932	0.41105	0.14892	0.05619	0.00247	0.9	350	107	352	15
Y15-16-21	meta	48.9	48.8	1.00	0.05171	0.02002	0.38390	0.14781	0.05383	0.00248	0.9	330	108	338	15
Y15-16-22	meta	11.9	83.9	0.14	0.05381	0.01495	0.40011	0.11051	0.05392	0.00192	0.9	342	80	339	12
Y15-16-23	meta	29.9	36.3	0.82	0.05312	0.01864	0.41106	0.14339	0.05611	0.00248	0.9	350	103	352	15
Y15-16-24	meta	28.0	32.7	0.86	0.05432	0.02047	0.46005	0.17261	0.06141	0.00256	0.9	384	120	384	16
Granulite Y18-4															
Y18-4-01	meta	12.1	23.8	0.51	0.05364	0.00642	0.46630	0.05531	0.06304	0.00130	0.9	389	38	394	8
Y18-4-02	meta	7.8	75.4	0.10	0.05590	0.00206	0.48715	0.01734	0.06319	0.00080	0.9	403	12	395	5
Y18-4-03	meta	18.1	28.5	0.63	0.05411	0.00464	0.47424	0.04018	0.06355	0.00113	0.9	394	28	397	7
Y18-4-04	meta	14.4	26.7	0.54	0.05501	0.00522	0.47126	0.04407	0.06212	0.00128	0.9	392	30	389	8
Y18-4-05	meta	11.1	69.1	0.16	0.05381	0.00212	0.46684	0.01783	0.06291	0.00082	0.9	389	12	393	5
Y18-4-06	meta	28.3	42.5	0.67	0.05382	0.00486	0.45693	0.04067	0.06156	0.00118	0.9	382	28	385	7
Y18-4-07	meta	15.0	28.8	0.52	0.05547	0.00477	0.47313	0.04015	0.06185	0.00111	0.9	393	28	387	7
Y18-4-08	meta	14.4	28.5	0.51	0.05553	0.00459	0.47322	0.03838	0.06179	0.00126	0.9	393	26	387	8
Y18-4-09	meta	16.4	36.4	0.45	0.05281	0.00324	0.44997	0.02708	0.06179	0.00097	0.9	377	19	387	6
Y18-4-10	meta	15.7	27.6	0.57	0.05294	0.00673	0.45307	0.05703	0.06206	0.00137	0.9	379	40	388	8
Y18-4-11	meta	5.7	73.9	0.08	0.05337	0.00266	0.45542	0.02215	0.06187	0.00092	0.9	381	15	387	6
Y18-4-12	meta	14.9	27.2	0.55	0.05527	0.00568	0.48474	0.04929	0.06360	0.00121	0.9	401	34	397	7
Y18-4-13	meta	14.2	27.6	0.51	0.05541	0.00463	0.46861	0.03855	0.06133	0.00115	0.9	390	27	384	7
Y18-4-14	meta	20.1	39.0	0.52	0.05550	0.00383	0.46985	0.03192	0.06139	0.00100	0.9	391	22	384	6
Y18-4-15	meta	11.1	21.3	0.52	0.05341	0.00561	0.45415	0.04707	0.06166	0.00136	0.9	380	33	386	8
Y18-4-16	meta	16.2	27.4	0.59	0.05405	0.01047	0.47234	0.09120	0.06337	0.00131	0.9	393	63	396	8
Y18-4-17	meta	14.4	26.3	0.55	0.05546	0.00594	0.48800	0.05175	0.06380	0.00122	0.9	404	35	399	7
Y18-4-18	meta	15.4	28.8	0.54	0.05527	0.00745	0.47483	0.06346	0.06230	0.00129	0.9	395	44	390	8
Y18-4-19	meta	12.1	114.8	0.11	0.05408	0.00203	0.46392	0.01689	0.06220	0.00081	0.9	387	12	389	5
Y18-4-20	meta	8.7	85.2	0.10	0.05541	0.00226	0.47547	0.01878	0.06223	0.00085	0.9	395	13	389	5
Y18-4-21	meta	18.4	33.5	0.55	0.05437	0.00385	0.47636	0.03318	0.06353	0.00110	0.9	396	23	397	7
Y18-4-22	meta	10.4	21.6	0.48	0.05550	0.00556	0.47396	0.04695	0.06193	0.00119	0.9	394	32	387	7
Y18-4-23	meta	12.0	21.9	0.55	0.05570	0.00472	0.48299	0.04032	0.06287	0.00120	0.9	400	28	393	7
Y18-4-24	meta	22.1	34.1	0.65	0.05352	0.00510	0.46320	0.04364	0.06276	0.00111	0.9	386	30	392	7
Y18-4-25	meta	13.7	26.7	0.51	0.05484	0.00600	0.47106	0.05081	0.06229	0.00148	0.9	392	35	390	9

Note: meta, metamorphic zircon.

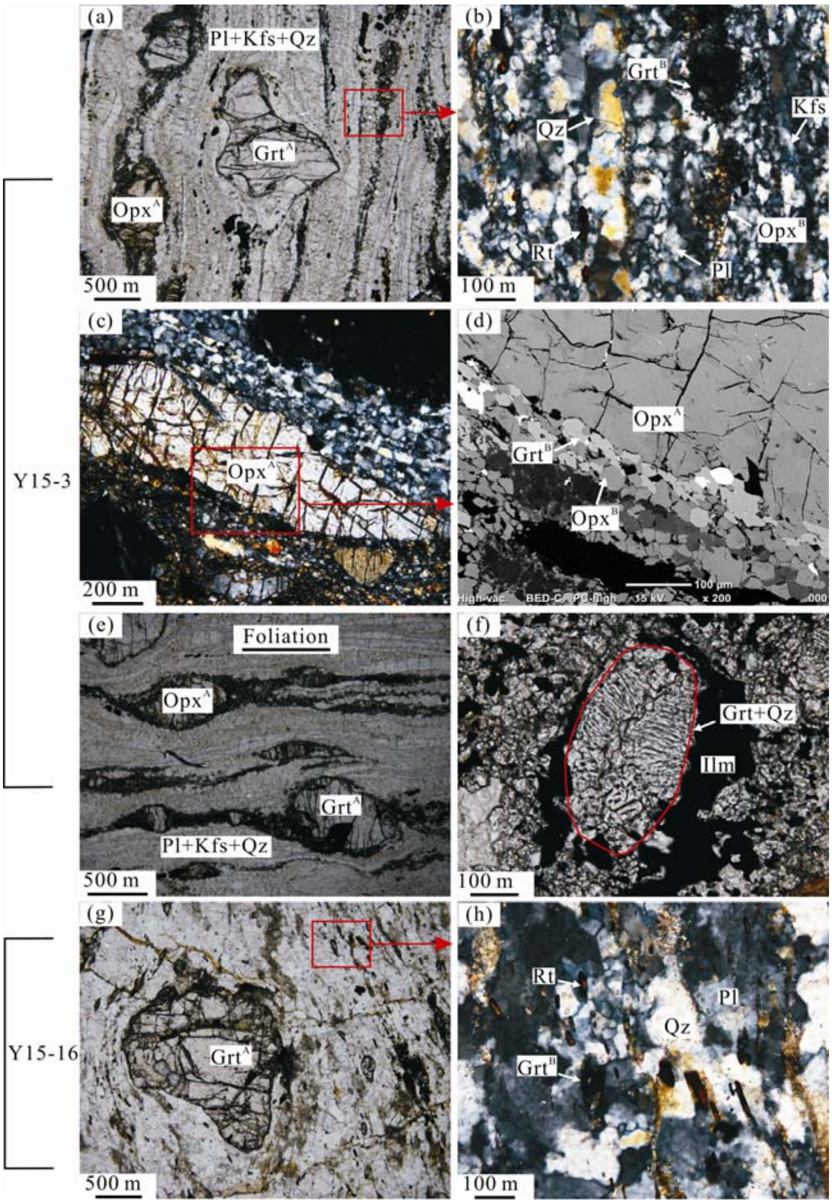

Fig. 3. Photomicrographs showing textural relationship of the Yushugou felsic granulites.

(a), Porphyroblastic garnet (Grt^A, 0.5-1 mm in diameter) and orthopyroxene (Opx^A, 0.5-1 mm in diameter). (b), Matrix minerals which consist mainly of fine-grained garnet (Grt^B) and orthopyroxene (Opx^B), plagioclase, K-feldspar, quartz, rutile and ilmenite; sample Y15-3. (c,d), Small grained garnet were found around the Opx^A; sample Y15-3. (e), The HP felsic granulites from Yushugou show distinct mylonitic foliation; sample Y15-3. (f), The intergrowth of grt and quartz (probably pseudomorphs after orthopyroxene); sample Y15-3. (g,h), Porphyroblastic garnet (1 mm in size, denoted as Grt^A) is distributed in a matrix which consist mainly of fine-grained garnet (denoted as Grt^B), quartz, plagioclase, rutile and ilmenit; sample Y15-16. Mineral abbreviations: qz, quartz; rt, rutile; ilm, ilmenite; other abbreviations are the same as in Fig.2.

5 Results

5.1 Mineral chemistry

5.1.1 Garnet

Garnet from two representative samples Y15-3 and Y15-16 generally exhibits compositional zoning. Grt^A from Type I opx-bearing felsic granulite sample Y15-3 exhibits two-stage compositional zoning (Table 2; Fig.4a,c), the CaO-poor and MgO-rich cores ($Alm_{50-52}Prp_{40-42}Grs_{5-6}Sps_1$) are characterized by almost constant grossular, pyrope, almandine and spessartine, while the rims ($Alm_{50-53}Prp_{38-40}Grs_{6-11}Sps_1$) show a subtle increase in the grossular content and decrease in the pyrope content. Grt^B ($Alm_{51-54}Prp_{34-40}Grs_{6-11}Sps_1$) displays a chemical zonation characterized by a CaO-rich and MgO-poor rim, comparable to the rims of Grt^A (Fig. 4a, d).

In Type II opx-free felsic granulite Y15-16, Grt^A also shows a two-stage compositional zoning (Table 2; Fig. 4b, e): the CaO-poor and MgO-rich cores ($Alm_{48-50}Prp_{40-41}Grs_{6-7}Sps_{2-3}$) are characterized by almost constant grossular, pyrope, almandine and spessartine, while the rims ($Alm_{47-50}Prp_{36-40}Grs_{7-13}Sps_{2-3}$) show a subtle increase

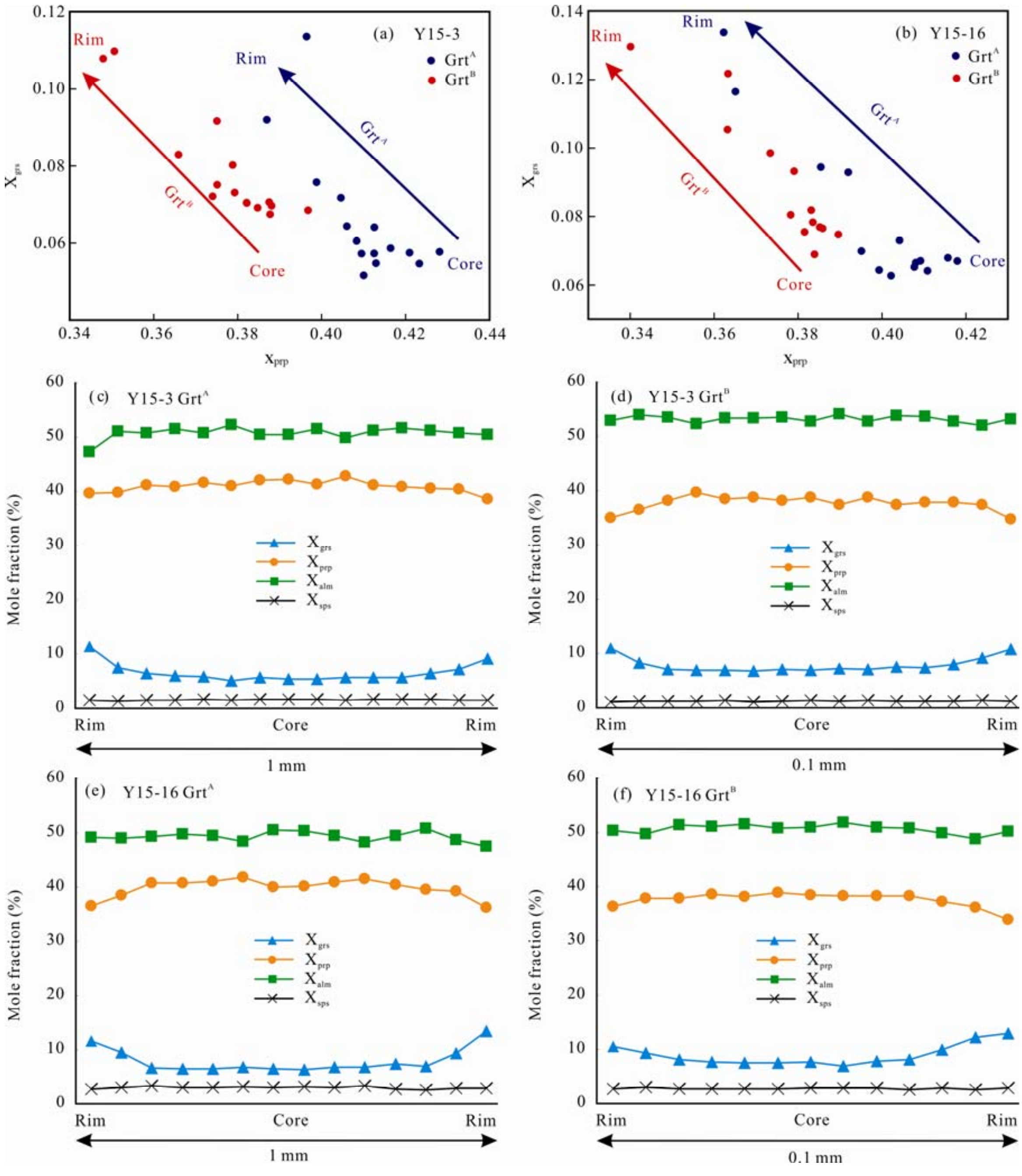

Fig. 4. Mineral chemistry diagrams showing variations of garnet in the felsic granulites from Yushugou.
(a,b), X_{prp}-X_{grs} diagrams showing core-rim variations (arrows) of garnet in Type I felsic granulite (Y15-3) and Type II felsic granulite (Y15-16), respectively. (c,d), Compositional profiles of garnet Grt^A and Grt^B in Y15-3. (e, f), Compositional profiles of garnet Grt^A and Grt^B in Y15-16. X_{grs} = Ca/(Ca + Mg + Fe^{2+} + Mn), X_{prp} = Mg/(Ca + Mg + Fe^{2+} + Mn), X_{alm} = Fe^{2+}/(Ca + Mg + Fe^{2+} + Mn), X_{sps} = Mn/(Ca + Mg + Fe^{2+} + Mn).

in the grossular content and decrease in the pyrope content. Grt^B ($Alm_{48-52}Prp_{34-39}Grs_{7-13}Sps_{2-3}$) displays a chemical zonation characterized by a CaO-rich and MgO-poor rim, comparable to the rims of Grt^A (Fig. 4b, f).

5.1.2 Other minerals

In Type I opx-bearing felsic granulite Y15-3, the X_{an} (=Ca/(Ca + Na)) of plagioclase ranges from 0.36–0.38, belongs to andesine. Opx^A and Opx^B have similar X_{Mg} (= Mg/(Mg + Fe^{2+})) between 0.65–0.69, which belongs to hypersthene. Opx^A shows a subtle decrease in the Al_2O_3 content (5.12–2.22 wt%) from core to rim, which may indicate temperature decreasing or pressure increasing. The Al_2O_3 content of Opx^B (1.76–2.56 wt%) is similar or less than Opx^A. The X_{Mg} and TiO_2 contents of biotite range from 0.75–0.82 and 4.30–8.06 wt%, respectively.

In Type II opx-free felsic granulite Y15-16, the X_{an} of plagioclase ranges from 0.34–0.38 and belongs to

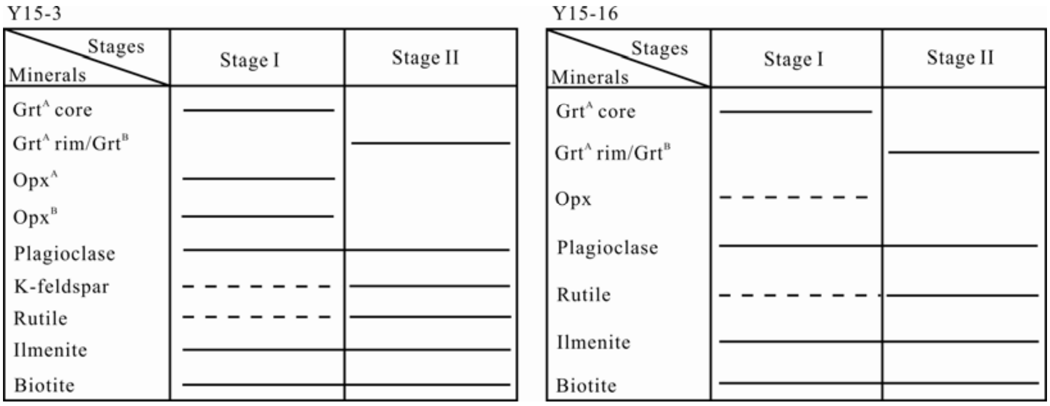

Fig. 5. Distinct mineral assemblages developed during different metamorphic stages in felsic granulites Y15-3 and Y15-16.
The metamorphic stages and the names on top of the lines represent the different stages of the minerals, which can be recognized according to different compositions and textures. Continuous lines represent minerals still present in the sample, whereas dashed lines indicate inferred minerals.

andesine. The X_{mg} and TiO_2 contents of biotite range from 0.67–0.75 and 3.01–6.10 wt% respectively.

Based on the textural observations and mineral compositions, the observed assemblages in the felsic granulites Y15-3 and Y15-16 can be related to two stages in this metamorphic evolution. A summary of mineral parageneses related to different stages of metamorphisms is presented in Fig. 5.

5.2 Phase equilibrium modelling

Phase equilibrium modelling was performed using the software THERMOCALC 3.33 (Powell et al., 1998; updated July 2009) and the November 2003 updated version of the Holland and Powell (1998) dataset (file tcds55.txt). P-T pseudosections were constructed for granulites Y15-3 and Y15-16 in the model system Na_2O-CaO-K_2O-FeO-MgO-SiO_2-H_2O-TiO_2-O (NCKFMASHTO). Activity–composition relationships are those presented for garnet (White et al., 2007), orthopyroxene (White et al., 2002), plagioclase (Holland and Powell, 2003), biotite (White et al., 2007), muscovite (Coggon and Holland, 2002), k-feldspar (Holland and Powell, 2003), liquid (White et al., 2007), cordierite (Holland and Powell, 1998), ilmenite (White et al., 2000). Rutile, kyanite, quartz and H_2O are treated as pure end-member phases. The H_2O content used in the modelling is adjusted using T-M (H_2O) diagrams and refers to the normalized molar proportion of H_2O in a rock (Korhonen et al., 2012). The whole-rock chemical compositions obtained by XRF analysis for calculating the pseudosections were normalized in the NCKFMASHTO system, the bulk Fe_2O_3 (O) contents were estimated by integrating the modal abundances of all phases relevant in the model systems with their charge balance. For the Stage I granulite facies metamorphism, the XRF-based whole-rock compositions were regarded as effective bulk compositions during the initial growth of garnet cores. However, the bulk-rock composition may change during its P-T evolution due to crystal fractionation (such as zoned garnet) (Evans, 2004; Du et al., 2014) and occasional presence of mineral enriched and mineral depleted textural domains (Wei et al., 2009; Groppo and Castelli, 2010). Therefore, it is critical to generate an effective bulk composition for phase equilibrium calculations. For Stage II granulite facies metamorphism, the bulk composition may not necessarily involve entire mineral grains (Carson et al., 1999; Wei et al., 2003), effective bulk-rock compositions were generated following the method of Carson et al. (1999) and Du et al. (2014) by integrating mineral compositions and modal abundance data for the phases present.

5.2.1 P-T pseudosections for the opx-bearing granulite Y15-3

The NCKFMASHTO P-T pseudosection calculated for the opx-bearing granulite Y15-3, using XRF-based bulk composition (Table 1), which is presented in Fig. 6a. The pseudosection is contoured with isopleths of z(g) = Ca/(Ca + Mg + Fe^{2+}) and x(g) = Fe^{2+}/(Fe^{2+} + Mg) contents in garnet. The measured core compositions of Grt^A correspond to P-T conditions of 9.8–10.2 kbar and 895–915°C in the stability field of grt + pl + bt + kfs + ilm + qz + liq (± opx), consistent with the Stage I metamorphic mineral assemblages observed under the microscope (details see part 4).

The NCKFMASHTO P-T pseudosection shown in Fig. 6b was calculated for Y15-3 with an effective bulk-rock composition obtained by subtracting Opx^A composition and the core of Grt^A composition from the XRF-based bulk-rock composition (Table 2) and is contoured with isopleths of z(g) and x(g). The measured Grt^B core-rim

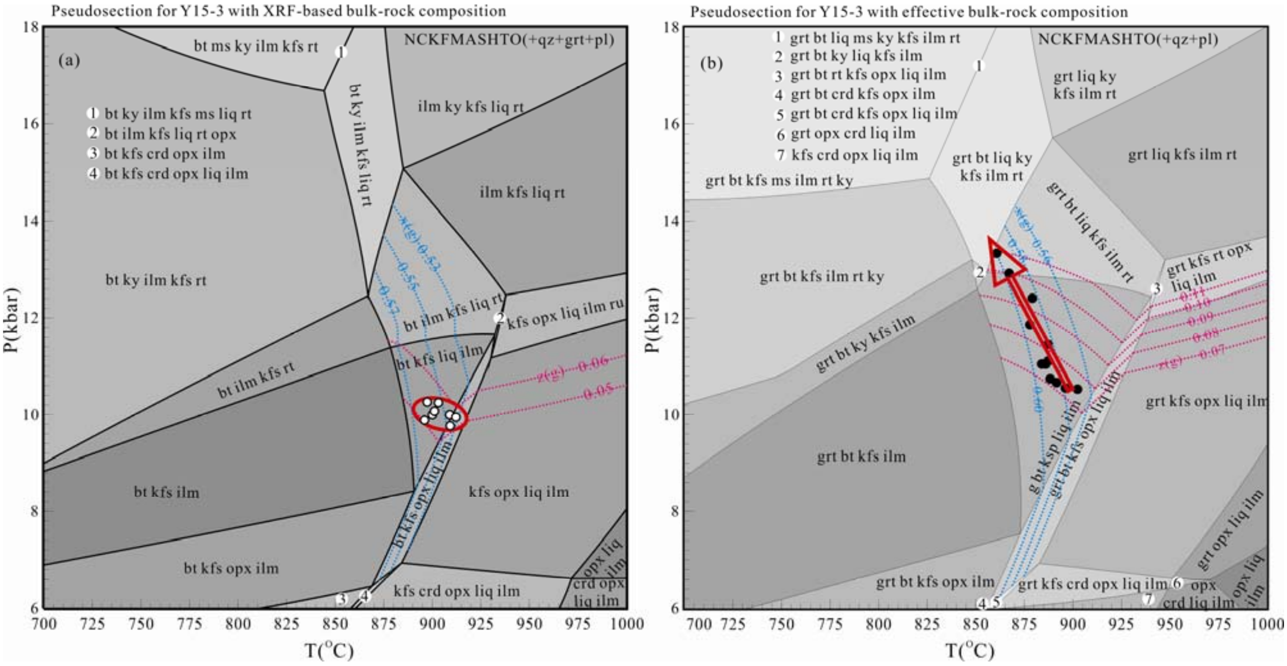

Fig. 6. P-T pseudosections for the Yushugou HP felsic granulite Y15-3 in the system NCKFMASHTO.

(a), P-T pseudosection for Stage I of Type I felsic granulite (sample Y15-3) calculated in the system NCKFMASHTO (+ qz + grt + pl) using the bulk-rock composition from Table 1, normalized on the basis of mole percent as SiO_2 = 65.27, Al_2O_3 = 10.11, TiO_2 = 0.94, CaO = 3.45, MgO = 7.05, FeO = 8.24, K_2O = 1.28, Na_2O = 1.98, H_2O = 1.28. (b), P-T pseudosection for Stage II of Type I felsic granulite (sample Y15-3) calculated in the system NCKFMASHTO (+ qz + pl) using an effective bulk composition obtained by subtracting Opx^A composition and the core of Grt^A composition from the XRF-based bulk composition, normalized on the basis of mole percent as SiO_2 = 67.24, Al_2O_3 = 9.93, TiO_2 = 0.98, CaO = 4.11, MgO = 5.27, FeO = 6.42, K_2O = 1.34, Na_2O = 2.47, H_2O = 1.66. The pseudosections are contoured with isopleths of z (grt) = Ca/(Ca+Mg+Fe^{2+}) and x (grt) = Fe^{2+}/(Fe^{2+}+Mg) contents in garnet. White circles represent the core of Grt^A. Black circles represent Grt^B and the rim of Grt^A. Mineral abbreviations: qz, quartz; rt, rutile; ilm, ilmenite; bt, biotite; ms, muscovite; ky, kyanite; liq, silicate liquid/melt; crd, cordierite; other abbreviations are the same as in Fig.2.

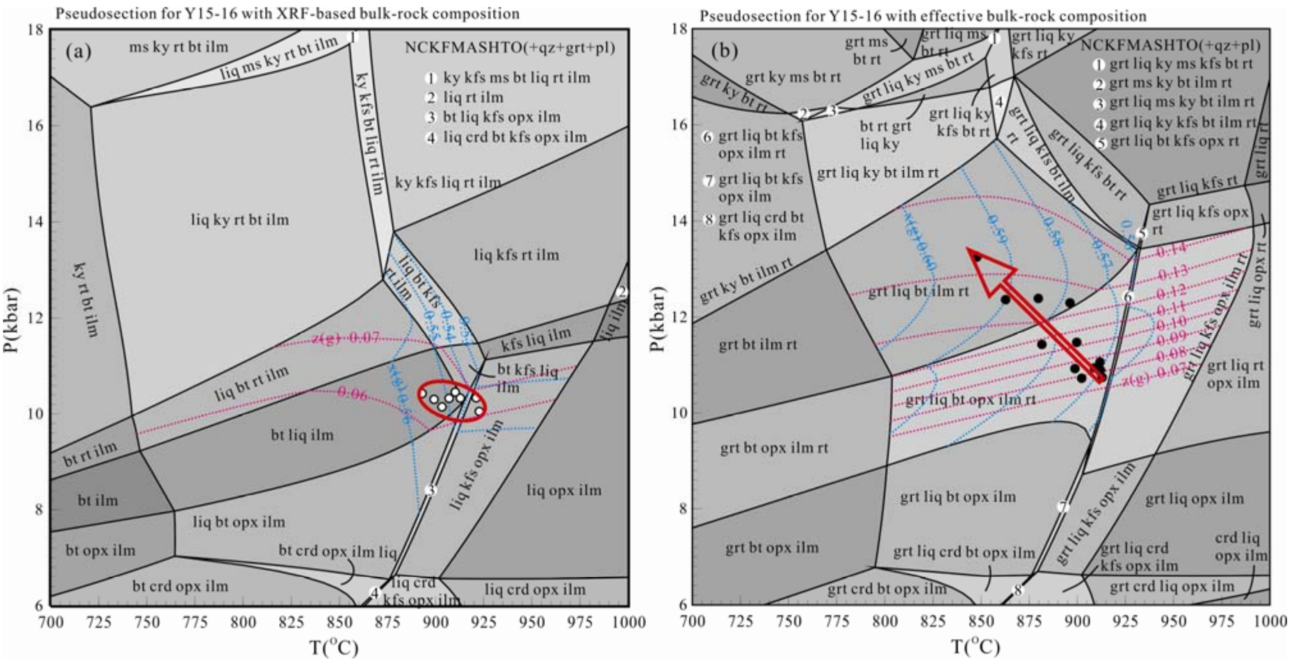

Fig. 7. P-T pseudosections for the Yushugou HP felsic granulite Y15-16 in the system NCKFMASHTO.

(a), P-T pseudosection for Stage I of Type II felsic granulite (sample Y15-16) calculated in the system NCKFMASHTO (+ qz + grt + pl) using the bulk-rock composition from Table 1, normalized on the basis of mole percent as SiO_2 = 80.87, Al_2O_3 = 5.26, TiO_2 = 0.45, CaO = 1.81, MgO = 4.32, FeO = 5.61, K_2O = 0.27, Na_2O = 0.74, H_2O = 0.47. (b), P-T pseudosection for Stage II of Type II felsic granulite (sample Y15-16) calculated in the system NCKFMASHTO (+ qz + pl) using an effective bulk composition obtained by subtracting the core of Grt^A composition from the XRF-based bulk composition, normalized on the basis of mole percent as SiO_2 = 81.95, Al_2O_3 = 4.99, TiO_2 = 0.85, CaO = 1.97, MgO = 3.66, FeO = 4.53, K_2O = 0.32, Na_2O = 1.12, H_2O = 0.51. White circles represent the core of Grt^A. Black circles represent Grt^B and the rim of Grt^A. Other details are the same as in Fig.6.

zoning (compositions similar with Grt^A rim zoning) is modelled to yield a P-T vector from 10.6 kbar, 900°C to 13.5 kbar, 860°C. P_{max} is in mineral assemblage of grt + pl + bt + kfs + rt + ilm + qz + liq. Phase equilibrium modelling indicate that sample Y15-3 has experienced an anticlockwise P-T path, suggesting a metamorphic process characterized by temperature decreasing and pressure increasing from 9.8–10.2 kbar and 895–915°C to 13.5 kbar, 860°C.

5.2.2 P-T pseudosections for the opx-free granulite Y15-16

The P-T pseudosection calculated for sample Y15-16 using the analysed bulk-rock composition (XRF method) is presented in Fig. 7a, the pseudosection is contoured with isopleths of z(g) and x(g). The measured core compositions of Grt^A yield P-T conditions of 10.0–10.4 kbar and 895–920°C in the stability field of grt + pl + bt + ilm + qz + liq (± opx ± kfs), similar with that in Fig. 6a.

The P-T pseudosection calculated with the effective bulk composition of sample Y15-16 is shown in Fig. 7b and contoured with isopleths of z(g) and x(g). The weakly zoned garnet grain (Grt^B) in the matrix is modelled to indicate a P-T vector from 10.7 kbar, 910°C to 13.2 kbar, 845°C, similar to sample Y15-3. The mineral assemblage of P_{max} is grt + pl + bt + rt + ilm + qz + liq. Thermodynamic modelling for sample Y15-16 suggests that it also experienced an anticlockwise P-T path from 10.0–10.4 kbar, 895–920°C to 13.2 kbar, 845°C, similar with that of sample Y15-3.

5.3 U-Pb zircon dating

Zircons from Type I felsic granulite Y15-3 and Y15-8 are oval in shape with grain sizes ranging from 100 to 200 μm in diameter and are transparent and colorless under transmitted light (Fig. 8). Cathodoluminescence (CL) study shows that zircons from sample Y15-3 posses core-rim structure, the dark-luminescent core surrounded by a narrow bright-luminescent rim (Fig. 8). Some of the cores preserve regular oscillatory zoning indicative for an igneous origin, while no zoning was observed in the rims suggest for a metamorphic origin. For sample Y15-8, no oscillatory zoning was founded in the zircons, all of them are featured by typical metamorphic origin. A few inclusions of quartz, feldspar, apatite and rutile were found in the metamorphic zircons. Six analyses of zircon oscillatory zoning cores from sample Y15-3 yield a weighted mean $^{206}Pb/^{238}U$ age of 430.6 ± 9.4 Ma (MSWD = 0.13; Fig. 9), which is interpreted to represent the time the zircon cores crystallized from magma chamber. 38 analyses of metamorphic zircons from Y15-3 yield two stage metamorphic ages which are 390.9 ± 4.1 Ma (n=34, MSWD = 0.14; Fig. 9) and 350.0 ± 12.0 Ma (n=4, MSWD = 0.03; Fig. 9) respectively. 50 analyses of zircons from sample Y15-8 yield a weighted mean $^{206}Pb/^{238}U$ age of 392.2 ± 1.6 Ma (MSWD = 0.44; Fig. 9).

The zircons from Type II felsic granulite Y15-16 and Y18-4 are also oval and colorless with 100–200 μm in major dimension. On CL images, most zircons are featured by typical multi-facet of metamorphic origin (Vavra et al., 1999; Wu and Zheng, 2004). A few inclusions of quartz, apatite and rutile were found in zircons from sample Y15-16 and Y18-4, while some zircons from Y18-4 also contain feldspar and garnet. 16 analysis on zircons from sample Y15-16 give a weighted mean $^{206}Pb/^{238}U$ age of 389.6 ± 6.5 Ma (MSWD = 0.29; Fig. 9), while eight analysis on zircons yielded a weighted mean $^{206}Pb/^{238}U$ age of 341.6 ± 7.0 Ma (MSWD = 0.48; Fig. 9). For sample Y18-4, 25 analysis on zircons yield a weighted mean $^{206}Pb/^{238}U$ age of 390.5 ± 2.6 Ma (MSWD = 0.44; Fig. 9).

6 Discussion

6.1 Metamorphic evolution of HP felsic granulite from South Tianshan

Previous research paid much attention to petrological investigations on the mafic granulite because of lacking appropriate method for felsic granulite. They use conventional geothermobarometry to calculate the pressure-temperature (P-T) conditions of the mafic granulite. The calculated peak P-T conditions of the mafic granulite are 800–870°C at 8.8–11.3 kbar (Shu Liangshu et al., 2004), 795–964°C at 9.7–14.2 kbar for the high pressure granulite facies (Grt-Di-Pl ± Qz assemblage) (Wang et al., 1999b), and 724–826°C at 6.4–8.8 kbar for the medium pressure granulite facies (Grt-Opx-Di-Pl-Qz assemblage) (Li Tianfu et al., 2011). More recently, Zhang et al. (2016) proposed that the felsic granulite underwent UHT (T>930°C) and HP (10.5–14.5 kbar) metamorphism by thermodynamic modelling.

Phase equilibrium modelling and petrological investigations have been carried out on the HP felsic granulite in Yushugou granulite-peridotite complex and yielded two stages metamorphic evolutionary with Stage I, the peak-temperature metamorphic stage and Stage II, which reach P_{max} after T_{max} by cooling processes.

Peak-temperature metamorphic stage I has been inferred on the basis of the Grt^A core compositions. The P-T conditions at the T_{max} stage were modelled to be 9.8-10.2 kbar at 895–915°C for Type I granulite sample Y15-3 and 10.0–10.4 kbar at 895–920°C for Type II granulite sample Y15-16. The corresponding mineral assemblage is grt + pl + bt + kfs + ilm + qz + liq (± opx) in the system

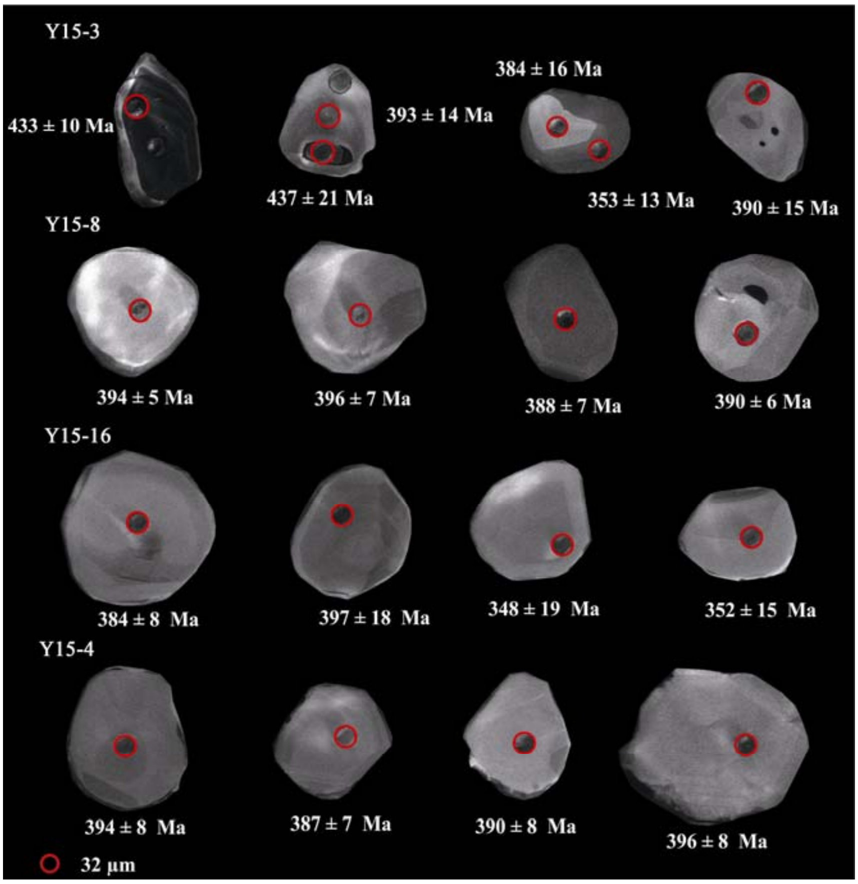

Fig. 8. Representative CL images of zircons from samples from Yushugou felsic granulite. Analytical spots, measured ages are marked.

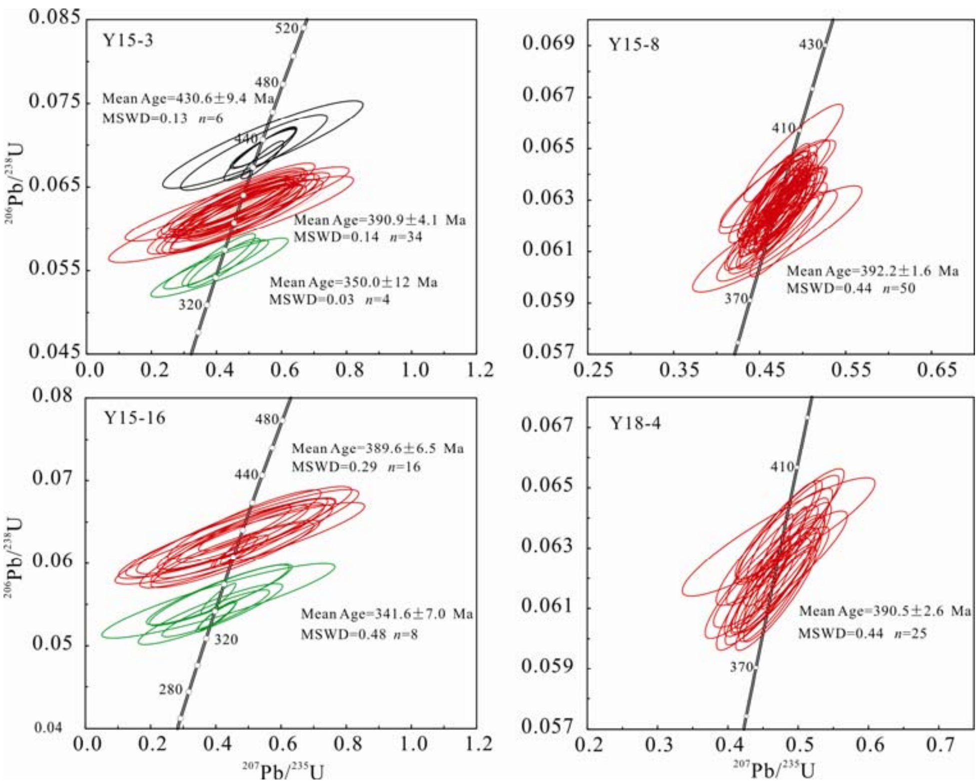

Fig. 9. Concordia diagrams for the investigated zircons from two types of felsic granulite in Yushugou granulite-peridotite complex.

NCKFMASHTO for Y15-3 and grt + pl + bt + ilm + qz + liq (± opx ± kfs) for Y15-16. The peak metamorphic temperature of the Yushugou granulite acquired in this study is higher than that calculated by traditional thermobarometry, but slightly lower than that proposed by Zhang et al. (2016). The calculated P-T conditions of the Yushugou HP felsic granulite imply a high geothermal gradient of ~26 ° C/km, distinct with HP/UHP metamorphic rocks in subduction and collision zones which are characterized by low geothermal gradient (4–15 °C/km; Chopin, 2003; Zhang et al., 2003; Liou et al., 2009; Gilotti, 2013). The post-T_{max} cooling and pressure increasing to the P_{max} stage II were constrained by the garnet growth zoning with increase in X_{grs} and decrease in X_{py}, which occurs from core to rim for most matrix garnet (Grt^B) or in rim of porphyroblastic garnet (Grt^A) in the two representative felsic granulite samples. The P-T conditions at the P_{max}, estimated using the garnet rim compositions with maximum X_{grs} and the corresponding X_{py}, are 13.5 kbar at 860°C for Y15-3 and 13.2 kbar at 845°C for Y15-16. The corresponding mineral assemblage is grt + pl + bt + kfs + rt + ilm + qz + liq for Y15-3 and grt + pl + bt + rt + ilm + qz + liq for Y15-16 in the system NCKFMASHTO. The changes in mineral mode suggest that orthopyroxene will disappear during pressure increasing through reaction: opx + pl = grt + qz, which is consistent with the reaction texture observed under microscope (Fig. 3c, d, f).

6.2 Zircon age interpretation

Different kinds of geochronological approaches have been used to constrain the age of the granulite from the Yushugou complex. Zhou et al. (2004) and Li Tianfu et al. (2011) use SHRIMP U-Pb method to acquire similar metamorphic ages which are 390–392 Ma and 390–401 Ma, respectively. The Sm-Nd isochron age of the granulites are 315 ± 3.62 Ma and 310 ± 5 Ma measured by Wang Runsan et al. (1999a) and Wang Runsan et al. (2003). The ^{40}Ar-^{39}Ar isochron ages of amphibolite from the granulite are 368.2 ± 4.8 Ma and 360 ± 10 Ma acquired by Wang Runsan et al. (2003).

In this study, the zircon U-Pb ages for zircons from two types of HP felsic granulites described above reveal three distinct age groups: Middle Silurian (~430 Ma), Middle Devonian (~390 Ma), Early Carboniferous (340–350 Ma). The inner cores of some zircons from sample Y15-3 preserve regular oscillatory zoning (Fig. 8) indicate a magmatic origin and give a weighted mean $^{206}Pb/^{238}U$ age of 430.6 ± 9.4 Ma, which is similar to the result of Wang et al. (1997). The second group of zircons from Y15-3, Y15-8, Y15-16 and Y18-4 give the weighted mean $^{206}Pb/^{238}U$ age of 390.9 ± 4.1 Ma, 392.2 ± 1.6 Ma, 389.6 ± 6.5 Ma and 390.5 ± 2.6 Ma, which correspond to peak-temperature metamorphic stage. This is consistent with the previous results that measured by SHRIMP zircon U-Pb isotopic dating method (Zhou et al., 2004; Li Tianfu et al., 2011). The third group of zircons from Y15-3 and Y15-16 give the weighted mean $^{206}Pb/^{238}U$ age of 350.0 ± 12 Ma and 341.6 ± 7 Ma, which may represent the post-T_{max} cooling and pressure increasing to the P_{max} stage metamorphism.

6.3 Tectonic implications

Based on the occurrence of HP-UHP belt together with discovery of coeval low-P granulite-facies rocks to the north, a paired metamorphic belt tectonic model is proposed for Chinese southwestern Tianshan and supposed to have formed owing to subduction of the South Tianshan Paleo-Ocean underneath the Yili and Central Tianshan plate (Li Qiang and Zhang Lifei, 2004; Zhang et al., 2007; Xia et al., 2014a; Lü and Zhang, 2016). The subduction of the South Tianshan Paleo-Ocean underneath the Yili and Central Tianshan plate may start at Early Silurian and last until Early Carboniferous (Gao et al., 2008; Han et al., 2011; Xia et al., 2014a; Xia et al., 2014b), which created a magmatic arc along the South margin of the Yili and Central Tianshan plate (Yang Tiannan et al., 2006; Zhu Yongfeng et al., 2006; Zhu Zhixin et al., 2006; Yang and Zhou, 2009; Zhu et al., 2009; Xu Xueyi et al., 2010; Long et al., 2011; Xu et al., 2013; Ma et al., 2014; Zhou et al., 2016).

The Yushugou HP granulite was traditionally considered to be deformed ophiolite slice (Wang Juli et al., 1999; Wang Runsan et al., 1999a; Wang et al., 1999b; Zhou et al., 2004). Geochemistry studies indicate that the protolith of the mafic granulite probably formed in a volcanic island arc tectonic setting (Shu Liangshuet al., 2004). Yang Jingsui et al. (2011) indicated that the Yushugou and Tonghuashan ophiolitic units originated in both MORB and SSZ tectonic settings, but the granulites appear to have had a complex protolith and a very different metamorphic history from the ophiolite. Ji Shaocheng et al. (2014) argued that this HP massif may derive from Moho transition zone and exhumated to surface through shearing action. Zhang et al. (2016) proposed that the Yushugou granulites probably derived from the deep root of a hot continental magmatic arc.

An anticlockwise P-T path was proposed for the Yushugou granulites in this study (Fig. 10). Stage I represent T_{max} granulite facies metamorphism which imply a high geothermal gradient of ~26 °C/km. This indicates that the felsic granulite can not be derived from the subducting slab which are characterized by low geothermal gradient (4–15 °C/km). We proposed that the

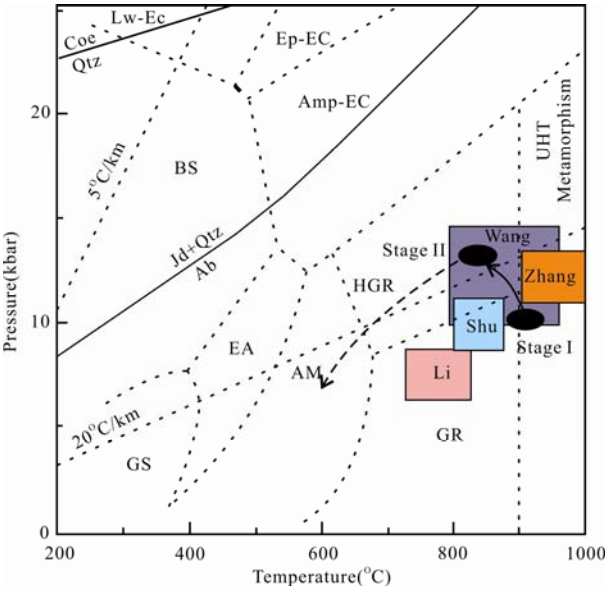

Fig. 10. Simplified P-T diagram with the P-T path derived in this study (arrowed lines).
Stage I granulite facies metamorphism happened at ~390 Ma and the P-T conditions are 9.8-10.4 kbar, 895-920 ℃; Stage II HP granulite facies metamorphism happened at 340-350 Ma and the P-T conditions are 13.2-13.5 kbar, 845-860 ℃. Symbols and boundaries of metamorphic facies follow Liou et al. (2004). The line that marks off UHT (ultra-high-temperature) metamorphism is referred to Harley (2008). Zhang, Wang, Shu and Li refer to the P-T conditions for the granulite from Zhang et al. (2016), Wang et al. (1999b), Shu Liangshu et al. (2004) and Li Tianfu et al. (2011), respectively.

Stage I granulite facies metamorophism happened at ~390 Ma that may be related to the Devonian magmatic arc (Han et al., 2011). Stage II HP granulite facies metamorphism took place at 340–350 Ma indicating the granulites have experienced a cooling and pressure increasing process, which may be related to the subduction erosion (Hacker et al., 2011; Gerya and Stöckhert, 2006). We propose a model for this process: the granulite was derived from the deep root of the hanging wall; Stage I granulite facies metamorphism happened at ~390 Ma, which may be related to the Devonian arc magmatic intrusion; Stage II HP granulite facies metamorphism (happened at 340–350 Ma) may be due to the involvement of granulite into the subducting slab and caused the pressure increasing and temperature decreasing.

7 Conclusions

(1) The studied high-pressure felsic granulites can be further grouped into two types: Type I (opx-bearing) and Type II (opx-free) granulite. Petrographic observations and phase equilibrium modelling with pseudosections calculated using THERMOCALC in the NCKFMASHTO system for two representative samples suggest that the granulites have experienced two stages of metamorphism: Stage I (granulite facies) was recognized by the porphyroblastic garnet core, and the P-T conditions of this stage are 9.8–10.2 kbar at 895–915°C for Type I and 10.0–10.4 kbar at 895–920° C for Type II granulite, respectively; Stage II (HP granulite facies) was based on the garnet zoning with increasing grossular and decreasing pyrope contents, and the P-T conditions of this stage, defined using the garnet rim compositions, are 13.5 kbar at 860°C for Type I and 13.2 kbar at 845°C for Type II granulite. Consequently, the Yushugou HP granulite has recorded an anticlockwise P-T path with temperature decreasing and pressure increasing simultaneously.

(2) The studies of zircon show that the protolith's ages of HP granlulites are ~430 Ma, the metamorphic rims of zircon have two group ages ~390 Ma and 340–350 Ma, corresponding to Stage I and II metamorphic events respectively.

(3) In this study, we propose a hanging wall subduction model for the HP graulites metamorphism based on the petrological study and U-Pb zircon dating: the granulite was derived from the deep root of the hanging wall; Stage I granulite facies metamorphism happened at ~390 Ma, which may be related to the Devonian arc magmatic intrusion; Stage II HP granulite facies metamorphism (happened at 340–350 Ma) may be due to the involvement of granulite into the subducting slab and caused the pressure increasing and temperature decreasing.

Acknowledgements

We greatly thank Prof. Chunjing Wei and Shuguang Song for their helpful discussions. We also thank Xiaoli Li for assistance with microprobe analyses and Fang Ma for zircon LA-ICP-MS dating. We also thank Huanglu Yu for his help in the field. This study was financially supported by the National Natural Science Foundation of China (Grants 41330210, 41520104004).

Manuscript recived Jan. 18, 2017
accepted Mar. 27, 2017
edited by Fei Hongcai

References

Allen, M.B., Windley, B.F., and Zhang, C., 1992. Palaeozoic collisional tectonics and magmatism of the Chinese Tien Shan, central Asia. *Tectonophysics*, 220(1–4): 89–115.

Andersen, T., 2002. Correction of common lead in U-Pb analyses that do not report Pb-204. *Chemical Geology*, 192(1–2): 59–79.

Appel, P., Möller, A., and Schenk, V., 1998. High-pressure granulite facies metamorphism in the pan-african belt of eastern tanzania: p–T–t evidence against granulite formation by continent collision. *Journal of Metamorphic Geology*, 16 (4): 491–509.

Carson, C.J., Powell, R., and Clarke, G.L., 1999. Calculated mineral equilibria for eclogites in CaO-Na_2O-FeO-MgO-Al_2O_3-SiO_2-H_2O: application to the Poue´bo Terrane, Pam Peninsula, New Caledonia. *Journal of Meramorphic Geology*, 17: 9–24.

Carswell, D.A., and O'Brien, P.J., 1993. Thermobarometry and geotectonic significance of high-pressure granulites: examples from the moldanubian zone of the bohemian massif in lower austria. *Journal of Petrology*, 34(3): 427–459.

Chopin, C., 2003. Ultrahigh-pressure metamorphism: tracing continental crust into the mantle. *Earth and Planetary Science Letters*, 212(1–2): 1–14.

Coggon, R., and Holland, T.J.B., 2002. Mixing properties of phengitic micas and revised garnet-phengite thermobarometers. *Journal of Metamorphic Geology*, 20(7): 683–696.

Coleman, R.G., 1989. Continental growth of northwest china. *Tectonics*, 8(3): 621–635.

Du, J.X., Zhang, L.F., Bader, T., Chen, Z.Y., and Lü, Z., 2014. Metamorphic evolution of relict lawsonite-bearing eclogites from the (U) HP metamorphic belt in the Chinese southwestern Tianshan. *Journal of Metamorphic Geology*, 32 (6): 575–598.

Evans, T.P., 2004. A method for calculating effective bulk composition modification due to crystal fractionation in garnet -bearing schist: implications for isopleth thermobarometry. *Journal of Metamorphic Geology*, 22(6): 547–557.

Gao, J., Klemd, R., Zhang, L., Wang, Z., and Xiao, X., 1999. P–t path of high-pressure/low-temperature rocks and tectonic implications in the western tianshan mountains, nw china. *Journal of Metamorphic Geology*, 17(6): 621–636.

Gao, J., Li, M.S., Xiao, X.C., Tang, Y.Q., and He, G.Q., 1998. Paleozoic tectonic evolution of the tianshan orogen, northwestern china. *Tectonophysics*, 287(1–4): 213–231.

Gao, J., Long, L.L., Klemd, R., Qian, Q., Liu, D.Y., Xiong, X.M., Su, W., Liu, W., Wang, Y.T., and Yang, F.Q., 2008. Tectonic evolution of the South Tianshan orogen and adjacent regions, NW China: geochemical and age constraints of granitoid rocks. *International Journal of Earth Sciences*, 98 (6): 1221–1238.

Gerya, T. and Stöckhert, B., 2006. Two-dimensional numerical modeling of tectonic and metamorphic histories at active continental margins. *International Journal of Earth Sciences*, 95(2): 250-274.

Gilotti, J.A., 2013. The Realm of Ultrahigh-Pressure Metamorphism. *Elements*, 9(4): 255–260.

Green, D.H., and Ringwood, A.E., 1967. An experimental investigation of the gabbro to eclogite transformation and its petrological applications. *Geochimica et Cosmochimica Acta*, 31(5): 767–833.

Groppo, C., and Castelli, D., 2010. Prograde P-T Evolution of a Lawsonite Eclogite from the Monviso Meta-ophiolite (Western Alps): Dehydration and Redox Reactions during Subduction of Oceanic FeTi-oxide Gabbro. *Journal of Petrology*, 51(12): 2489–2514.

Guo, J.H., O'Brien, P.J., and Zhai, M., 2002. High‐pressure granulites in the sanggan area, north china craton: metamorphic evolution, p–t paths and geotectonic significance. *Journal of Metamorphic Geology*, 20(20): 741–756.

Hacker, B.R., Kelemen, P.B., and Behn, M.D., 2011. Differentiation of the continental crust by relamination. *Earth and Planetary Science Letters*, 307(3–4): 501-516.

Han, B.F., He, G.Q., Wang, X.C., and Guo, Z.J., 2011. Late Carboniferous collision between the Tarim and Kazakhstan–Yili terranes in the western segment of the South Tian Shan Orogen, Central Asia, and implications for the Northern Xinjiang, western China. *Earth-Science Reviews*, 109(3–4): 74–93.

Harley, S.L., 1989. The origins of granulites: a metamorphic perspective. *Geological Magazine*, 126(03): 215–247.

Harley, S.L., 2008. Refining the P–T records of UHT crustal metamorphism. *Journal of Metamorphic Geology*, 26(2): 125–154.

Holland, T., and Powell, R., 2003. Activity-composition relations for phases in petrological calculations: an asymmetric multicomponent formulation. *Contributions to Mineralogy and Petrology*, 145(4): 492–501.

Holland, T.J.B., and Powell, R., 1998. An internally consistent thermodynamic data set for phases of petrological interest. *Journal of Metamorphic Geology*, 16(3): 309–343.

Huang He, Wang Tao, Qin Qie, Hou Jiyao, Tong Ying and Guo Lei, 2015. Zircon Hf isotopic characteristics of granitoids from the Baluntai region, Central Tianshan: implications for tectonic evolution and continental growth. *Acta Geologica Sinica*, 89(12): 2286–2313 (in Chinese with English abstract).

Ji Shaocheng, Wang Qian, Shao Tongbin, Sun Shengsi, Li Awei, Michibayashi Katsuyoshi, Kondo Yosuke and Li Jianfeng, 2014. The Yushugou granulite-peridotite terrane as a Paleozoic continental crust-mantle transition zone exposed at the northern margin of the southern Tianshan (Xinjiang). *Geotectonica et Metallogenia*, 38(3): 473–494 (in Chinese with English abstract).

Korhonen, F.J., Powell, R., and Stout, J.H., 2012. Stability of sapphirine+quartz in the oxidized rocks of the Wilson Lake terrane, Labrador: calculated equilibria in NCKFMASHTO. *Journal of Metamorphic Geology*, 30(1): 21–36.

Li Qiang and Zhang Lifei, 2004. The P-T path and geological significance of low-pressure granulite-facies metamorphism in Muzhaerte, southwest Tianshan. *Acta Petrologica Sinica*, 20 (3): 583–594 (in Chinese with English abstract).

Li Tianfu, Yang Jingsui, Ren Yufeng, Chen Songyong and Xu Xiangzhen, 2011. Metamorphism process and SHRIMP dating of granulite at Yushugou, northern margin of South Tianshan. *Acta Petrologica Sinica*, 27(1): 147–165 (in Chinese with English abstract).

Liou, J.G., Tsujimori, T., Zhang, R.Y., Katayama, I., and Maruyama, S., 2004. Glohal UHP Metamorphism and Continental subduction/collision: The Himalayan Model. *International Geology Review*, 46(1): 1–27.

Liou, J.G., Ernst, W.G., Zhang, R.Y., Tsujimori, T., and Jahn, B.M., 2009. Ultrahigh-pressure minerals and metamorphic terranes – The view from China. *Journal of Asian Earth Sciences*, 35(3-4): 199–231.

Long, L.L., Gao, J., Klemd, R., Beier, C., Qian, Q., Zhang, X., Wang, J.B., and Jiang, T., 2011. Geochemical and geochronological studies of granitoid rocks from the Western Tianshan Orogen: Implications for continental growth in the southwestern Central Asian Orogenic Belt. *Lithos*, 126(3-4): 321–340.

Lü, Z., and Zhang, L.F., 2016. Differential evolution of high-pressure and ultrahigh-pressure metapelites from Habutengsu, Chinese Western Tianshan: phase equilibria modelling and

$^{40}Ar/^{39}Ar$ geochronology. *Acta Geologica Sinica* (English edition), 90(2): 628–640.

Lü, Z., Zhang, L.F., Du, J.X., and Bucher, K., 2008. Coesite inclusions in garnet from eclogitic rocks in western Tianshan, northwest China: Convincing proof of UHP metamorphism. *American Mineralogist*, 93(11–12): 1845–1850.

Lü, Z., Zhang, L.F., Du, J.X., Yang, X., Tian, Z.L., and Xia, B., 2012. Petrology of HP metamorphic veins in coesite-bearing eclogite from western Tianshan, China: Fluid processes and elemental mobility during exhumation in a cold subduction zone. *Lithos*, 136–139: 168–186.

Ludwig, K.R., 2003. *User's Manual for Isoplot 3.0: a Geochronological Toolkit for Microsoft Excel*. Berkeley: Berkeley Geochronology Center Special Publication No.4, 71.

Ma, X.X., Shu, L.S., Meert, J.G., and Li, J.Y., 2014. The Paleozoic evolution of Central Tianshan: Geochemical and geochronological evidence. *Gondwana Research*, 25(2): 797–819.

O'Brien, P.J., and Rötzler, J., 2003. High-pressure granulites: formation, recovery of peak conditions and implications for tectonics. *Journal of Metamorphic Geology*, 21(1): 3–20.

Powell, R., Holland, T., and Worley, B., 1998. Calculating phase diagrams involving solid solutions via non-linear equations, with examples using THERMOCALC. *Journal of Metamorphic Geology*, 16(4): 577–588.

Shu Liangshu, Wang Ciyin and Ma Ruishi, 1996. Granulite relics and pyroxene- facies ductile deformation in the northern boundary of the southern Tianshan. *Scientia Geologica Sinica*, 31(4): 375–384 (in Chinese with English abstract).

Shu Liangshu, Yu Jinhai, Charvet, J., Laurent-Charvet, S., Sang Haiqing and Zhang Rengu, 2004. Geological, geochronological and geochemical features of granulites in the Eastern Tianshan, NW China. *Journal of Asian Earth Sciences*, 24(1): 25–41.

Sláma, J., Košler, J., Condon, D.J., Crowley, J.L., Gerdes, A., Hanchar, J.M., Horstwood, M.S.A., Morris, G.A., Nasdala, L., Norberg, N., Schaltegger, U., Schoene, B., Tubrett, M.N., and Whitehouse, M.J., 2008. Plešovice zircon - A new natural reference material for U–Pb and Hf isotopic microanalysis. *Chemical Geology*, 249(1–2): 1–35.

Smithies, R.H., and Bagas, L., 1997. High pressure amphibolite-granulite facies metamorphism in the paleoproterozoic rudall complex, central western australia. *Precambrian Research*, 83 (4): 243–265.

Vavra, G., Schmid, R., and Gebauer, D., 1999. Internal morphology, habit and U-Th-Pb microanalysis of amphibolite-to-granulite facies zircons: geochronology of the Ivrea Zone (Southern Alps). *Contributions to Mineralogy and Petrology*, 134(4): 380–404.

Wang Juli, Wang Rensan, Zhou Dingwu, Wang Yan and Liu Yangjie, 1999. A study of tectonites of granulite facies in Yushugou, South Tianshan, China. *Acta Petrologica Sinica*, 15 (4): 539–547 (in Chinese with English abstract).

Wang Runsan, Wang Juli, Zhou Dingwu, Wang Yan and Liu Yangjie, 1999a. Study on Yushugou ophiolite suite modified with the metamorphism of granulite facies in southern Tianshan. *Scientia Geologica Sinica*, 34(2): 166–176 (in Chinese with English abstract).

Wang Runsan, Wang Yan, Liu Yangjie, Yan Jincai and Wang Juli, 1997. The para-granulite in bedded complex from Yushugou, South Tianshan, Xinjiang Autonomous Region: Its petrological characteristics and geodynamic significance. *Journal of North West University* (Natural Science Edition), 27(5): 411–416 (in Chinese with English abstract).

Wang, R.S., Zhou, D.W., Wang, J.L., Wang, Y. and Liu, Y.J., 1999b. Variscan terrane of deep-crustal granulite facies in Yushugou area, southern Tianshan. *Science China Earth Sciences*, 42(5): 482–490.

Wang Runsan, Zhou Dingwu, Wang Yan, Wang Juli, Sang Haiqing and Zhang Renhu, 2003. Geochronology for the multiple-stage metamorphism of high-pressure terrane of granulite fades from yushugou area, south tianshan. *Acta Petrologica Sinica*, 19(3): 452–460 (in Chinese with English abstract).

Wang Yan, Wang Runsan, Zhou Dingwu and Wang Juli, 1999. A study of spinels from a granulite terrain in Yushugou, South Tianshan Mountain. *Acta Petrologica et Mineralogica*, 19(3): 247–254 (in Chinese with English abstract).

Wei Chunjing, 2012. Advance of metamorphic petrology during the first decade of the 21st century. *Bulletin of Mineralogy, Petrology and Geochemistry*, 31(5): 415–427 (in Chinese with English abstract).

Wei, C.J., Wang, W., Clarke, G.L., Zhang, L.F., and Song, S.G., 2009. Metamorphism of High/ultrahigh-pressure Pelitic-Felsic Schist in the South Tianshan Orogen, NW China: Phase Equilibria and P-T Path. *Journal of Petrology*, 50(10): 1973–1991.

Wei Chunjing, Zhang Cuiguang, Zhang Ali, Wu Tianhong and Li Jianghai, 2001. Metamorphic P-T conditions and geological significance of high-pressure granulite from the Jianping complex, western Liaoning province. *Acta Petrologica Sinica*, 17(2): 269–282 (in Chinese with English abstract).

Wei, C.J., Powell, R., and Zhang, L.F., 2003. Eclogites from the south Tianshan, NW China: petrological characteristic and calculated mineral equilibria in the Na_2O–CaO–FeO–MgO–Al_2O_3–SiO_2–H_2O system. *Journal of Meramorphic Geology*, 21: 163–179.

White, R.W., Powell, R., and Clarke, G.L., 2002. The interpretation of reaction textures in Fe-rich metapelitic granulites of the Musgrave Block, central Australia: constraints from mineral equilibria calculations in the system K_2O-FeO-MgO-Al_2O_3-SiO_2-H_2O-TiO_2-Fe_2O_3. *Journal of Metamorphic Geology*, 20(1): 41–55.

White, R.W., Powell, R., and Holland, T.J.B., 2007. Progress relating to calculation of partial melting equilibria for metapelites. *Journal of Metamorphic Geology*, 25(5): 511–527.

White, R.W., Powell, R., Holland, T.J.B., and Worley, B.A., 2000. The effect of TiO_2 and Fe_2O_3 on metapelitic assemblages at greenschist and amphibolite facies conditions: mineral equilibria calculations in the system K_2O–FeO–MgO–Al_2O_3–SiO_2–H_2O–TiO_2–Fe_2O_3. *Journal of Metamorphic Geology*, 18: 497–511.

Wiedenbeck, M., AllÉ, P., Corfu, F., Griffin, W.L., Meier, M., Oberli, F., Quadt, A.V., Roddick, J.C., and Spiegel, W., 1995. Three Natural Zircon Standards for U-Th-Pb, Lu-Hf, Trace Element And Ree Analyses. *Geostandards and Geoanalytical Research*, 19(1): 1–23.

Windley, B.F., Allen, M.B., Zhang, C., Zhao, Z.Y., and Wang, G.R., 1990. Paleozoic accretion and cenozoic redeformation of the chinese tien shan range, central asia. *Geology*, 18(2): 128.

Wu Wenkui, Jiang Changyi, Yang Fu and Li Liangchen, 1992. The Yushugou-Tonghuashan structural mixtite in Xinjiang. *Journal of Xi'an College of Geology*, 14(1): 8–13 (in Chinese with English abstract).

Wu, Y.B., and Zheng, Y.F., 2004. Genesis of zircon and its constraints on interpretation of U-Pb age. *Chinese Science Bulletin* (English edition), 49(15): 1554–1569.

XBGMR (Xinjiang Bureau of Geology and Mineral Resources), 1959. 1: 200,000 geological map of Kumux sheet (K-45-17).

XBGMR (Xinjiang Bureau of Geology and Mineral Resources), 1960. 1: 200,000 geological map of Baoertu sheet (K-45-16).

Xia, B., Zhang, L.F., and Bader, T., 2014a. Zircon U–Pb ages and Hf isotopic analyses of migmatite from the 'paired metamorphic belt' in Chinese SW Tianshan: Constraints on partial melting associated with orogeny. *Lithos*, 192–195: 158–179.

Xia, B., Zhang, L.F., Xia, Y., and Bader, T., 2014b. The tectonic evolution of the Tianshan Orogenic Belt: Evidence from U–Pb dating of detrital zircons from the Chinese southwestern Tianshan accretionary mélange. *Gondwana Research*, 25(4): 1627–1643.

Xu, X.Y., Wang, H.L., Li, P., Chen, J.L., Ma, Z.P., Zhu, T., Wang, N., and Dong, Y.P., 2013. Geochemistry and geochronology of Paleozoic intrusions in the Nalati (Narati) area in western Tianshan, Xinjiang, China: Implications for Paleozoic tectonic evolution. *Journal of Asian Earth Sciences*, 72: 33–62.

Xu Xueyi, Wang Hongliang, Ma Guolin, Li Ping, Chen Junlu and Li Ting, 2010. Geochronology and Hf isotope characteristics of the Paleozoic granite in Nalati area, West Tianshan Mountains. *Acta Petrologica et Mineralogica*, 29(6): 691–706 (in Chinese with English abstract).

Xu Xiangzhen, Yang Jingsui, Guo Guolin, Li Tianfu, Ren Yufeng and Chen Songyong, 2011. The Yushugou-Tonghuashan ophiolites in Tianshan, Xinjiang, and their tectonic setting. *Acta Petrologica Sinica*, 27(1): 96–120 (in Chinese with English abstract).

Yang Jingsui, Xu Xiangzhen, Li Tianfu, Chen Songyong, Ren Yufeng, Li Jinyang and Liu Zhao, 2011. U-Pb ages of zircons from ophiolite and related rocks in the Kumishi region at the southern margin of Middle Tianshan, Xinjiang: evidence of early Paleozoic oceanic basin. *Acta Petrologica Sinica*, 27(1): 77–95 (in Chinese with English abstract).

Yang, S.H., and Zhou, M.F., 2009. Geochemistry of the ~430-Ma Jingbulake mafic–ultramafic intrusion in Western Xinjiang, NW China: Implications for subduction related magmatism in the South Tianshan orogenic belt. *Lithos*, 113(1–2): 259–273.

Yang Tiannan, Li Jinyi, Sun Guihua and Wang Yanbin, 2006. Earlier Devonian active continental arc in Central Tianshan: evidence of geochemical analyses and zircon SHRIMP dating on mylonitized granitic rock. *Acta Petrologica Sinica*, 22(1): 41–48 (in Chinese with English abstract).

Yuan, H.L., Gao, S., Liu, X.M., Li, H.M., Günther, D., and Wu, F.Y., 2004. Accurate U–Pb age and trace element determinations of zircon by laser ablation-inductively coupled plasmamass spectrometry. *Geostandards and Geoanalytical Research*, 28: 353–370.

Zhai Mingguo, 2009. Two kinds of granulites (HT-HP and HT-UHT) in North China Craton: Their genetic ralation and geotectonic implications. *Acta Petrologica Sinica*, 25(8): 1753–1771 (in Chinese with English abstract).

Zhang, L.F., Ai, Y.L., Song, S.G., Liou, J., and Wei, C.J., 2007. A Brief Review of UHP Meta-ophiolitic Rocks, Southwestern Tianshan, Western China. *International Geology Review*, 49 (9): 811–823.

Zhang, L., Ellis, D.J., Arculus, R.J., Jiang, W., and Wei, C., 2003. 'Forbidden zone' subduction of sediments to 150km depth - the reaction of dolomite to magnesite + aragonite in the uhpm metapelites from western tianshan, china. *Journal of Metamorphic Geology*, 21(6): 523–529.

Zhang, L.F., Gao, J., Ekebair, S., and Wang, Z.X., 2001. Low temperature eclogite facies metamorphism in western tianshan, xinjiang. *Science China Earth Sciences*, 44(1): 85–96.

Zhang, L.F., Song, S.G., Liou, J.G., Ai, Y.L., and Li, X.P., 2005. Relict coesite exsolution in omphacite from Western Tianshan eclogites, China. *American Mineralogist*, 90(1): 181–186.

Zhang, L., Zhang, J.F., and Jin, Z.M., 2016. Metamorphic P–T–water conditions of the Yushugou granulites from the southeastern Tianshan orogen: Implications for Paleozoic accretionary orogeny. *Gondwana Research*, 29(1): 264–277.

Zhou, D.W., Li, S., Jian, P., Wang, R.S., Liu, X.M., Lu, G.X., and Wang, J.L., 2004. Zircon U-Pb SHRIMP ages of high-pressure granulite in Yushugou ophiolitic terrane in southern Tianshan and their tectonic implications. *Chinese Science Bulletin* (English edition), 49(13): 1415–1419.

Zhou, H., Chen, L., Sun, Y., and Zhu, T., 2016. Tectonic framework of late paleozoic intrusions in Xingxingxia: implications for final closure of South Tianshan ocean in East Tianshan. *Acta Geologica Sinica* (English edition), 90(2): 604–627.

Zhu, Y.F., Guo, X., Song, B., Zhang, L.F., and Gu, L.B., 2009. Petrology, Sr-Nd-Hf isotopic geochemistry and zircon chronology of the Late Palaeozoic volcanic rocks in the southwestern Tianshan Mountains, Xinjiang, NW China. *Journal of the Geological Society*, 166(6): 1085–1099.

Zhu Yongfeng, Zhou Jing and Guo Xuan, 2006. Petrology and Sr-Nd isotopic geochemistry of the Carboniferous volcanic rocks in the western Tianshan Mountains, NW China. *Acta Petrologica Sinica*, 22(5): 1341–1350 (in Chinese with English abstract).

Zhu Zhixin, Wang Kezhuo, Zheng Yujie, Sun Guihua, Zhang Chao and Li Yaping, 2006. Zircon SHRIMP dating of Silurian and Devonian granitic intrusions in the southern Yili block, Xinjiang and preliminary discussion on their tectonic setting. *Acta Petrologica Sinica*, 22(5): 1193–1200 (in Chinese with English abstract).

About the first author

LU Zhang, female, born in 1990 in Changzhi City, Shanxi province; PhD candidate, the Key Laboratory of Orogenic Belts and Crustal Evolution, Ministry of Education, School of Earth and Space Sciences, Peking University. She is now interested in the study on metamorphic geology. Email: zhanglu@pku.edu.cn; phone: 18811465275.